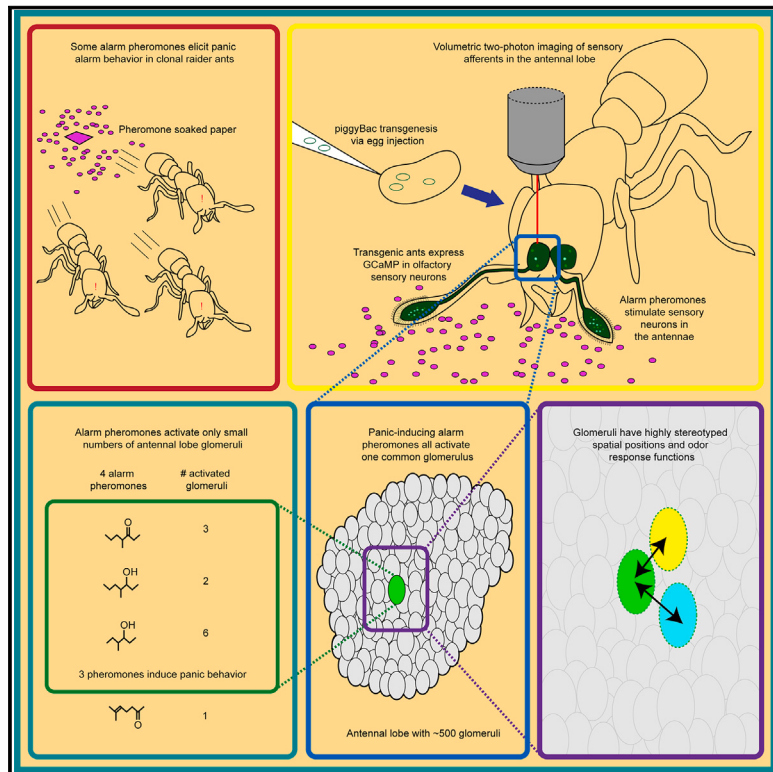


Sparse and stereotyped encoding implicates a core glomerulus for ant alarm behavior

Graphical abstract



Authors

Taylor Hart, Dominic D. Frank,
Lindsey E. Lopes, ..., Amelia Ritger,
Stephany Valdés-Rodríguez,
Daniel J.C. Kronauer

Correspondence

thart@rockefeller.edu (T.H.),
dkronauer@rockefeller.edu (D.J.C.K.)

In brief

A transgenesis method for the clonal raider ant, yielding expression of the genetically encoded calcium indicator GCaMP6s in all olfactory sensory neurons, has shown how ants use spatially precise encodings for alarm pheromones.

Highlights

- An efficient transgenesis method for the clonal raider ant
- Generation of a transgenic line expressing GCaMP6s in olfactory sensory neurons
- Calcium imaging reveals highly stereotyped odor encoding in the ant antennal lobe
- Alarm pheromones are sparsely encoded and activate a core glomerulus

Article

Sparse and stereotyped encoding implicates a core glomerulus for ant alarm behavior

Taylor Hart,^{1,*} Dominic D. Frank,¹ Lindsey E. Lopes,¹ Leonora Olivos-Cisneros,¹ Kip D. Lacy,¹ Waring Trible,^{1,2} Amelia Ritger,^{1,3} Stephany Valdés-Rodríguez,^{1,4} and Daniel J.C. Kronauer^{1,4,5,*}

¹Laboratory of Social Evolution and Behavior, The Rockefeller University, 1230 York Avenue, New York, NY 10065, USA

²John Harvard Distinguished Science Fellowship Program, Harvard University, 52 Oxford Street, NW Cambridge, MA 02138, USA

³Department of Ecology, Evolution, and Marine Biology, University of California, Santa Barbara, Marine Science Research Building, Bldg. 520, Santa Barbara, CA 93106, USA

⁴Howard Hughes Medical Institute, New York, NY 10065, USA

⁵Lead contact

*Correspondence: thart@rockefeller.edu (T.H.), dkronauer@rockefeller.edu (D.J.C.K.)

<https://doi.org/10.1016/j.cell.2023.05.025>

SUMMARY

Ants communicate via large arrays of pheromones and possess expanded, highly complex olfactory systems, with antennal lobes in the brain comprising up to ~500 glomeruli. This expansion implies that odors could activate hundreds of glomeruli, which would pose challenges for higher-order processing. To study this problem, we generated transgenic ants expressing the genetically encoded calcium indicator GCaMP in olfactory sensory neurons. Using two-photon imaging, we mapped complete glomerular responses to four ant alarm pheromones. Alarm pheromones robustly activated ≤ 6 glomeruli, and activity maps for the three pheromones inducing panic alarm in our study species converged on a single glomerulus. These results demonstrate that, rather than using broadly tuned combinatorial encoding, ants employ precise, narrowly tuned, and stereotyped representations of alarm pheromones. The identification of a central sensory hub glomerulus for alarm behavior suggests that a simple neural architecture is sufficient to translate pheromone perception into behavioral outputs.

INTRODUCTION

Eusocial insects, such as ants and honeybees, use vast arrays of pheromones to communicate information with conspecifics and to regulate colony life. These adaptations correspond to elaborations of the chemosensory system, which are particularly striking in ants. Insect olfactory systems have a conserved organization, with olfactory sensory neurons (OSNs) in peripheral sensory organs innervating glomeruli in the antennal lobes (ALs) in the brain.^{1–3} Much of the detailed knowledge of insect olfactory system development, anatomy, and neural function comes from studies of the vinegar fly, *Drosophila melanogaster*. However, ants express an order of magnitude more odorant receptor genes (ORs) in their antennae and possess an order of magnitude more AL glomeruli than *Drosophila*.^{4–14} In *Drosophila*, the ~50 AL glomeruli each receive input from a functional class of OSNs and have stereotyped positions across individuals, which allowed the creation of atlases mapping odor-evoked response functions for each glomerulus.^{2,15–18} By contrast, little is known about the wiring of OSN subpopulations, OR expression patterns at the level of individual OSNs, or how odors are represented in the more complex olfactory system of ants, which contains up to ~500 AL glomeruli.

Here, we focus on the neural representation of alarm pheromones, “danger” signals that are chemically well characterized across several ant species. Ant alarm pheromones are typically produced in the mandibular-, poison-, or Dufour’s gland and stored in a glandular reservoir. The pheromone is then released into the surrounding air in response to danger.¹⁹ Stimulating individuals with volatile alarm pheromones is experimentally simple and quickly elicits behavioral responses, which makes these pheromones attractive models for studying the neurobiological basis of chemical communication. Upon perception of the pheromone, locomotion usually increases, and the subsequent behavioral responses are often grouped into two major categories: “aggression” and “panic.”²⁰ Panic alarm responses involve fast movements either away from the alarm source or without a clear direction and can culminate in nest evacuation, where ants leave the nest carrying brood.^{20–22} Specific features of alarm behavior vary with context, species, and specific mixtures and concentrations of chemicals, and in addition to increased locomotor speed and alertness, can include changes in the posture of antennae, mandibles, and the sting.^{20,23,24}

Alarm pheromone representation has been investigated using calcium dyes to record activity from subsections of the AL in several carpenter ant species^{25–27} and honeybees.^{28–34} These studies found broad, multi-glomerular activation patterns

without evidence for specialized glomerulus clusters, similar to the combinatorial representation of general odorants in *Drosophila*.^{18,28,32,35–37} Such a combinatorial model, in which many glomeruli respond to a given odorant, implies that odor mixtures could potentially activate combinations of hundreds of glomeruli in the expanded ant AL. Because the number of potential combinations of glomeruli grows super-linearly with each additional glomerulus in the AL, this scenario poses much bigger challenges for higher-order neurons in ants vs. *Drosophila* with respect to decoding multicomponent olfactory signals, detecting and identifying pheromones, and activating appropriate behavioral responses. In contrast, if most odorants only activate a small number of glomeruli, this could simplify the neural architecture necessary for processing odor information in the complex olfactory environment of an ant colony and ensure that chemical signals can be rapidly and accurately perceived.

The ant olfactory system also differs from that of *Drosophila* in several developmental properties that might be linked to its increased complexity.^{11,12,38,39} Based on these differences, it has been suggested that ants, similar to mice but unlike flies, might rely on intrinsic features of ORs for OSN axon guidance and AL patterning.^{11,39} This in turn could translate to increased developmental plasticity in the olfactory system. In both mice and *Drosophila*, olfactory glomeruli receiving input from a defined class of OSNs are consistently located in the same anatomical region, but at the local scale, homologous mouse glomeruli vary substantially in their spatial position across individuals, and even across the left/right axis within a single individual.^{40–43} Whether the level of anatomical-functional stereotypy of the ant olfactory glomeruli more closely resembles *Drosophila* or mice has not been assessed. However, the number of glomeruli in ants varies with sex, caste, and worker body size,^{4,5,9,44} suggesting that stereotypy may be low.

We studied the representation of alarm pheromones in the clonal raider ant *Oceraea biroi*, an experimentally tractable species that lives in small colonies, reproduces asexually, and preys on other ants.^{12,45,46} We implemented neurogenetic tools in ants by developing a piggyBac transgenesis protocol to generate a line that expresses the genetically encoded calcium indicator GCaMP6s in OSNs. We then examined the relationship between behavioral outputs of alarm pheromone stimuli and single-glomerulus-resolution, whole-AL calcium responses for four ant alarm pheromones.

RESULTS

Alarm pheromones elicit a range of behavioral responses

The alarm pheromones 4-methyl-3-heptanone and 4-methyl-3-heptanol have previously been extracted from clonal raider ants and verified to elicit panic alarm responses, with ants rapidly leaving the nest pile and evacuating the nest chamber.²² These compounds induce panic both alone and as a 9:1 blend that mimics their relative abundance in ant head extracts (Figures 1A and 1B; Table S1).²² These pheromones are exclusively found in the head and likely derive from the mandibular gland.²² We decided to also study the effects of two alarm pheromones of other ant species, 4-methyl-3-hexanol and 6-methyl-

5-hepten-2-one. These compounds were not found in clonal raider ant chemical extracts but share chemical similarity to the clonal raider ant alarm pheromones (Figure 1A; Table S1).^{22,47–55} Because clonal raider ants are specialized predators of a variety of other ants,⁴⁶ they are likely exposed to the alarm pheromones of their prey species during raids, potentially including 4-methyl-3-hexanol and 6-methyl-5-hepten-2-one.

Using the same bioassay and analyses that we previously used to study 4-methyl-3-heptanone and 4-methyl-3-heptanol (Figure 1B),²² we characterized the behavioral response to 4-methyl-3-hexanol and 6-methyl-5-hepten-2-one. Both compounds caused ants to leave the initial nest pile and the initial nest chamber (Figures 1C and 1D). However, the behavioral responses were qualitatively distinct from one another, prompting additional analyses. Blinded categorization of the major behavioral response to each pheromone (see STAR Methods), including re-analysis of videos from our previous study,²² showed that 4-methyl-3-heptanone, 4-methyl-3-heptanol, the 4-methyl-3-heptanone/4-methyl-3-heptanol blend, and 4-methyl-3-hexanol all caused the ants to rapidly leave and disassemble the nest pile (which was defined as persisting as long as it contained at least one egg and two workers) within 1 min after exposure in at least 80% of trials. We call this response an “immediate panic alarm.” The most common response to 6-methyl-5-hepten-2-one was for the majority of ants to slowly walk away from the nest, while the nest pile persisted for more than 1 min. We call this response “ants leave nest” (Figure 1E; Video S1).

In many of our behavioral trials, the original nest pile was disassembled, which is consistent with nest evacuation as part of a panic alarm response. In other cases, the ants moved away from the nest pile while leaving it at least partially intact, which reflects a disturbance among the ants but not a clear evacuation or panic response. We analyzed the length of time that the original nest remained intact for each odorant and found that treatment with 4-methyl-3-hexanol led to similarly rapid disassembly of the nest as 4-methyl-3-heptanone, 4-methyl-3-heptanol, and the blend (Figure 1F; Table S2). In contrast, treatment with 6-methyl-5-hepten-2-one produced a wide range of outcomes, and the average response was significantly different from responses to clonal raider ant alarm pheromones (Figure 1F; Table S2).²² In summary, 4-methyl-3-hexanol elicits panic alarm behavior similar to the native clonal raider ant alarm pheromones 4-methyl-3-heptanone and 4-methyl-3-heptanol. 6-methyl-5-hepten-2-one, on the other hand, lacks panic alarm activity and does not normally cause nest evacuation. The occasional alarm responses to 6-methyl-5-hepten-2-one could represent secondary responses, in which an ant emits an actual alarm pheromone in response to the stimulus compound.

Creation of transgenic ants

GCaMP has been used to study olfaction in several insect species, including honeybees.^{18,56,57} We reasoned that targeting GCaMP to ant OSNs using a promoter from the odorant receptor co-receptor *Orco* could allow optical recording of neural activity in sensory afferents in the ALs, similar to other insects.^{18,56,58,59} We therefore cloned a 2.4 kb genomic fragment upstream of the *O. biroi* *Orco* gene, which presumably contained promoter and

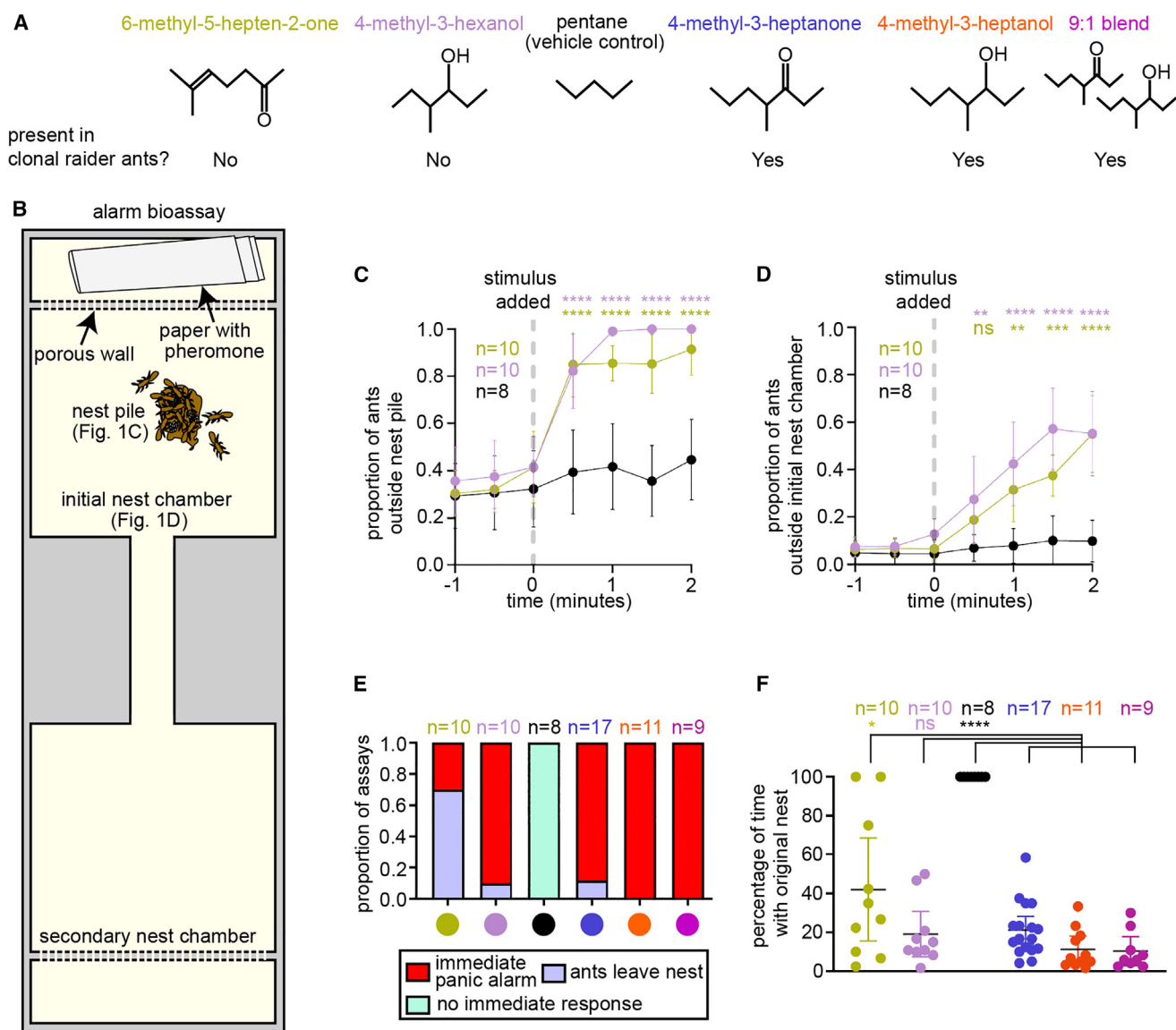


Figure 1. Behavioral responses to four ant alarm pheromones

(A) Chemical structures of four ant alarm pheromones and the vehicle control used in this study, obtained from the PubChem database (National Institute for Biotechnology Information: <https://pubchem.ncbi.nlm.nih.gov>).

(B) Experimental design for the colony alarm bioassay.²² The features used for analyses in (C) and (D) are indicated.

(C and D) Time series of colony responses to the alarm pheromones 6-methyl-5-hepten-2-one and 4-methyl-3-hexanol vs. control (mean \pm SEM). See Figure S2 for time series plots for 4-methyl-3-heptanone and 4-methyl-3-heptanol in wild-type and GCaMP6s ants.

(E) Categorical analysis of major behavioral responses to alarm pheromone stimuli.

(F) Quantification of the length of time that the original nest pile remained intact for the two minutes post stimulus in the bioassays from (C) and (D); mean \pm 95% CI; see Table S2 for details. * p < 0.05; ** p < 0.01; *** p < 0.001; **** p < 0.0001, compared with vehicle control for (C) and (D); non-*O. biroi* alarm pheromones and the vehicle control were compared with known *O. biroi* alarm pheromones for (F); see Table S2 for details. The color code for chemical compounds in (A) applies to all figure panels.

enhancer elements sufficient to drive specific expression in all clonal raider ant OSNs (fragment ObirOrco), following *Orco*'s expression pattern.^{11,12} We then constructed a piggyBac vector plasmid in which ObirOrco drives expression of GCaMP6s⁶⁰ using the QF2 and 15xQUAS binary expression driver and effector elements in tandem to amplify transgene expression (Fig-

ure 2A).⁶¹ Because we did not know if GCaMP6s would be detectable in live animals, we included an expression construct with the baculovirus-derived ie1 enhancer/promoter element to drive expression of the red fluorescent protein dsRed, based on similar designs used in other insects (Figure 2A).^{62–64} We injected ant eggs with a mix of plasmid DNA and transposase

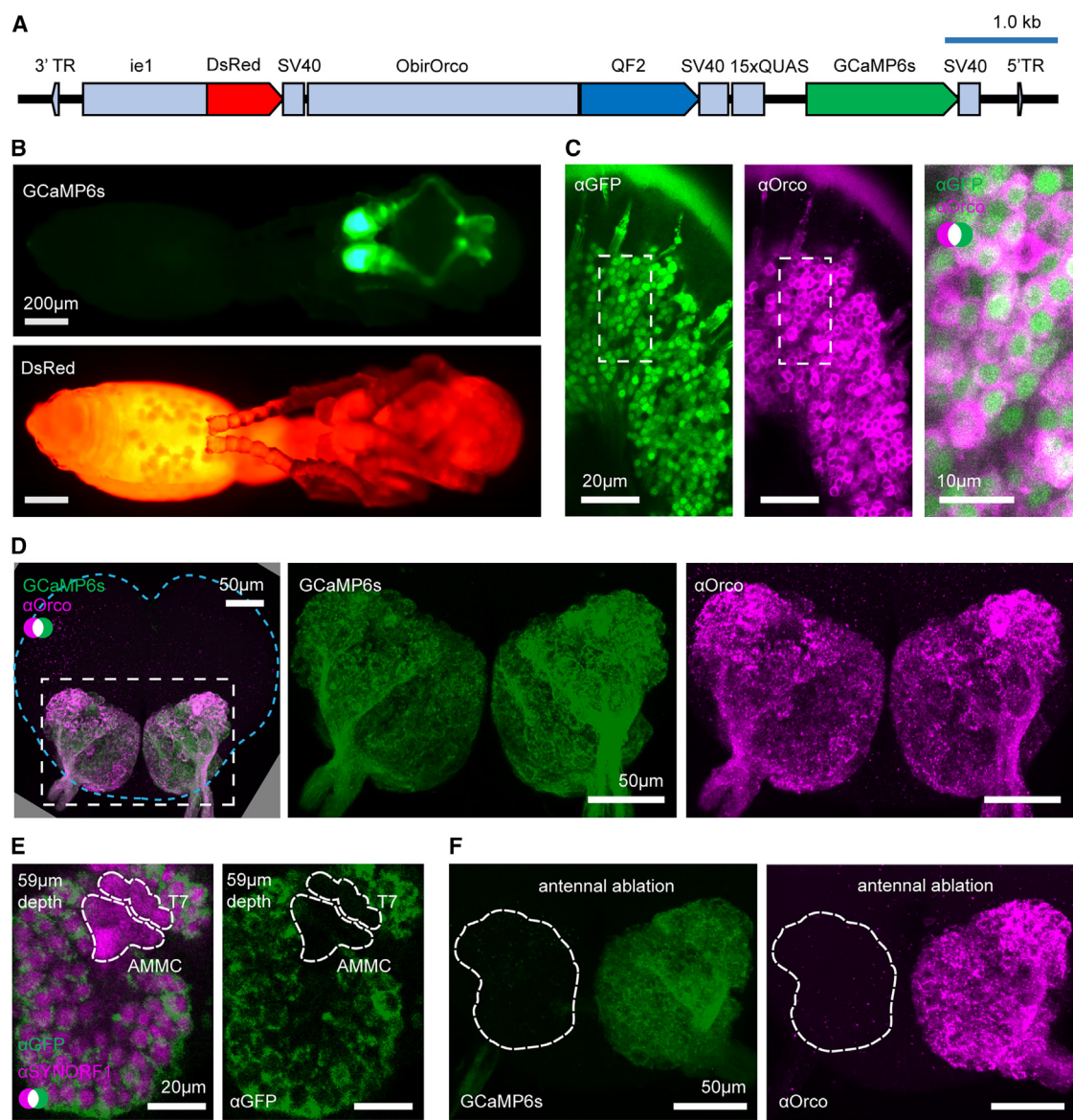


Figure 2. Transgene construct and GCaMP6s expression

(A) Construct design.

(B) Transgenic pupa under epifluorescence: GCaMP6s (top); dsRed (bottom); see [Figure S1](#) for comparisons with wild types.

(C) Anti-GFP (green, cytoplasmic) and anti-Orco (magenta, membrane bound) densely label OSNs in the antennal club (max z-projection through 3 1-μm slices).

(D) GCaMP6s and anti-Orco signal co-localize in the ALs (max z-projection through the AL); brain contour is shown with cyan line.

(E) Anti-SYNORF1 (magenta; neuropil) and anti-GFP (green) staining from a single optical slice in the AL. T7: T7 cluster of glomeruli; AMMC: antennal mechanosensory and motor center.

(F) Unilateral ablation of the antenna eliminates GCaMP6s (green, left) and anti-Orco signal (magenta, right) from the AL (max z-projections; white outline indicates the AL boundary as determined from phalloidin stain). See [Figures S1](#) and [S2](#) for additional characterization of GCaMP6s ant brains. See [Figure S3](#) for genomic analyses of GCaMP6s ants.

mRNA⁶⁵ and reared the resulting G0 individuals using protocols modified from Trible et al.¹² (see [STAR Methods](#) for details and [Table 1](#)). Although we generated several separate transgenic lines, we recovered a large and stable population only from one of them, which we used for all later experiments (first four rows, [Table 1](#)). Henceforth, we refer to these ants as “GCaMP6s ants.”

Characterization of transgenic ants

We characterized transgene expression in our transgenic line to determine if it would be useful for imaging odor-evoked calcium responses. Transgenic pupae had detectable GCaMP6s fluorescence in the antennae, consistent with expression in OSNs, and dsRed was broadly visible under epifluorescence ([Figures 2B](#) and [S1A](#)). dsRed is expressed at a low level in the ALs, possibly

Table 1. Generation of transgenic clonal raider ants expressing GCaMP6s

Treatment	$\frac{pmol}{\mu L}$ DNA	Egg age at injection (hours)	# eggs injected	# G0 eggs hatched	# G0 adults eclosed	# G0 adults with fluorescence	Minimum # of lines generated	Overall efficiency	Transformation efficiency
	$\frac{ng}{\mu L}$ RNA								
27.8/110	<5	1,945	155 (8.0%)	14	3	1	0.00021	0.026	
27.8/220	<5	1,367	72 (5.3%)	16	0				
27.8/440	<5	739	6 (0.8%)	0	0				
27.8/110	<3	637	15 (2.4%)	8	5				
27.8/110	<3	353	44 (12.5%)	17	2	1	0.0028	0.059	

The “treatment” column indicates injection mix concentrations of plasmid DNA and transposase mRNA. G0 adults from the first four treatments were reared as a group, and we therefore cannot determine which treatment generated the line that was propagated from that group. Overall efficiency was calculated by dividing the minimum number of lines generated by the number of eggs injected; transformation efficiency was calculated by dividing the minimum number of lines generated by the number of G0 adults eclosed.

due to leaky expression from ObirOrco (Figure S1B). We assessed GCaMP6s expression in OSNs in the antennal club using immunohistochemistry and found that GCaMP6s labels the great majority of Orco-positive cells (Figure 2C). In the ALs, high levels of GCaMP6s co-localized with Orco, which labels OSN afferents (Figure 2D).¹¹ GCaMP6s is also expressed in parts of the subesophageal zone and central complex (CC) (Figures S1C and S1D). These fluorescence patterns were all consistent across individuals.

To validate that our transgenic ants were good candidates for the study of AL function, we performed anatomical reconstructions of the ALs of two GCaMP6s ants using two different staining methods that label all brain neuropil. From the first AL, we reconstructed 505 glomeruli using anti-SYNORF1 signal (Figure S2A). From the second AL, using phalloidin, we reconstructed 508 glomeruli (Figure S2B). The total number of glomeruli is within the published range of wild-type ants (493–509 glomeruli),^{9,11,12} showing that the gross AL anatomy of the transgenic ants is normal. Next, we looked at the expression of GCaMP and Orco within the AL. Using our second reconstruction, which was co-stained with anti-Orco, we counted 502 Orco-positive glomeruli, all of which were also GCaMP6s-positive (Figure S2B). The 6 glomeruli of the T7 cluster were the only Orco-negative glomeruli, consistent with previous studies.^{9,11} A weak GCaMP6s signal was detected in 4 of the 6 T7 glomeruli (Figure S2B).

We then further investigated GCaMP expression using confocal images of brains stained with anti-GFP and anti-SYNORF1. Although glomeruli in T1–T6 were always robustly labeled by anti-GFP, the signal in the T7 glomeruli was consistently weaker than in other glomeruli and was often undetectable (Figure 2E). The antennal mechanosensory and motor center, another adjacent Orco-negative sensory structure,^{11,66} was consistently unlabeled by GCaMP6s or anti-GFP in our confocal stacks (Figure 2E). Together, this indicated that our transgenic line is a good candidate for detecting calcium responses from all olfactory glomeruli of the AL (about 99% of total glomeruli).

To see whether GCaMP6s is expressed by cells other than OSNs in the ALs, we performed unilateral antennal ablations on transgenic animals to sever the antennal nerve and examined their brains after allowing GCaMP6s and Orco to be cleared. Although GCaMP6s signal in the subesophageal zone and central complex

was unaffected (Figure S1E), GCaMP6s and anti-Orco signals were greatly reduced across the entire AL connected to the ablated antenna, and no clear glomerular labeling remained (Figure 2F). This indicates that GCaMP6s signal in the AL derives from the antennae and is likely to be exclusive to sensory neuron axons.

The expression of genetically encoded calcium indicators can alter cellular calcium buffering and affect behavior.^{67,68} We therefore examined whether the GCaMP6s ants had defects in alarm behavior by subjecting them to our alarm behavior bioassay. The ants left the nest cluster in response to 4-methyl-3-heptanone, 4-methyl-3-heptanol, and the blend, similar to wild types (Figures S2C and S2D). The effect on leaving the nest chamber was only significantly different from control for 4-methyl-3-heptanone and the blend (Figures S2E and S2F). Crucially, GCaMP6s ants perceive both alarm pheromones, and their behavioral response is qualitatively similar to wild types.

Finally, non-targeted transgene insertions can disrupt endogenous sequences,⁶⁹ and we therefore sequenced the genome of a GCaMP6s ant. The line contains a single, haploid transgene insertion on the 2nd chromosomal scaffold (Figures S3A and S3B). The insertion occurred at location Chr2:3,870,844–3,870,847, within an intron of the gene *trace amine-associated receptor 9* (Figure S3C). Because the insertion is haploid and not within a coding region, and because GCaMP6s animals have normal AL anatomy and robust behavioral responses, these animals are well suited for functional studies of the clonal raider ant olfactory system.

Recording calcium responses to general odorants

We developed an *in vivo* two-photon imaging preparation for clonal raider ants in which animals are head fixed and a small imaging window is excised from the cuticle covering the ALs (Figures 3A and 3B). Ants are then exposed to reproducible odor stimuli via a computer-controlled olfactometer,^{18,25,70} and the resulting changes in GCaMP6s fluorescence are captured at 27.5 fps, imaging the volume containing the entire AL every 1.2 s (33 z-planes at 5 μm increments; Figures 3C–3E; Video S2). Because most clonal raider ant glomeruli are 10–20 μm in diameter, they are all sampled in multiple imaging planes. Individual glomeruli were often discernible from baseline GCaMP6s fluorescence and always from calcium responses due to spatially clustered pixels

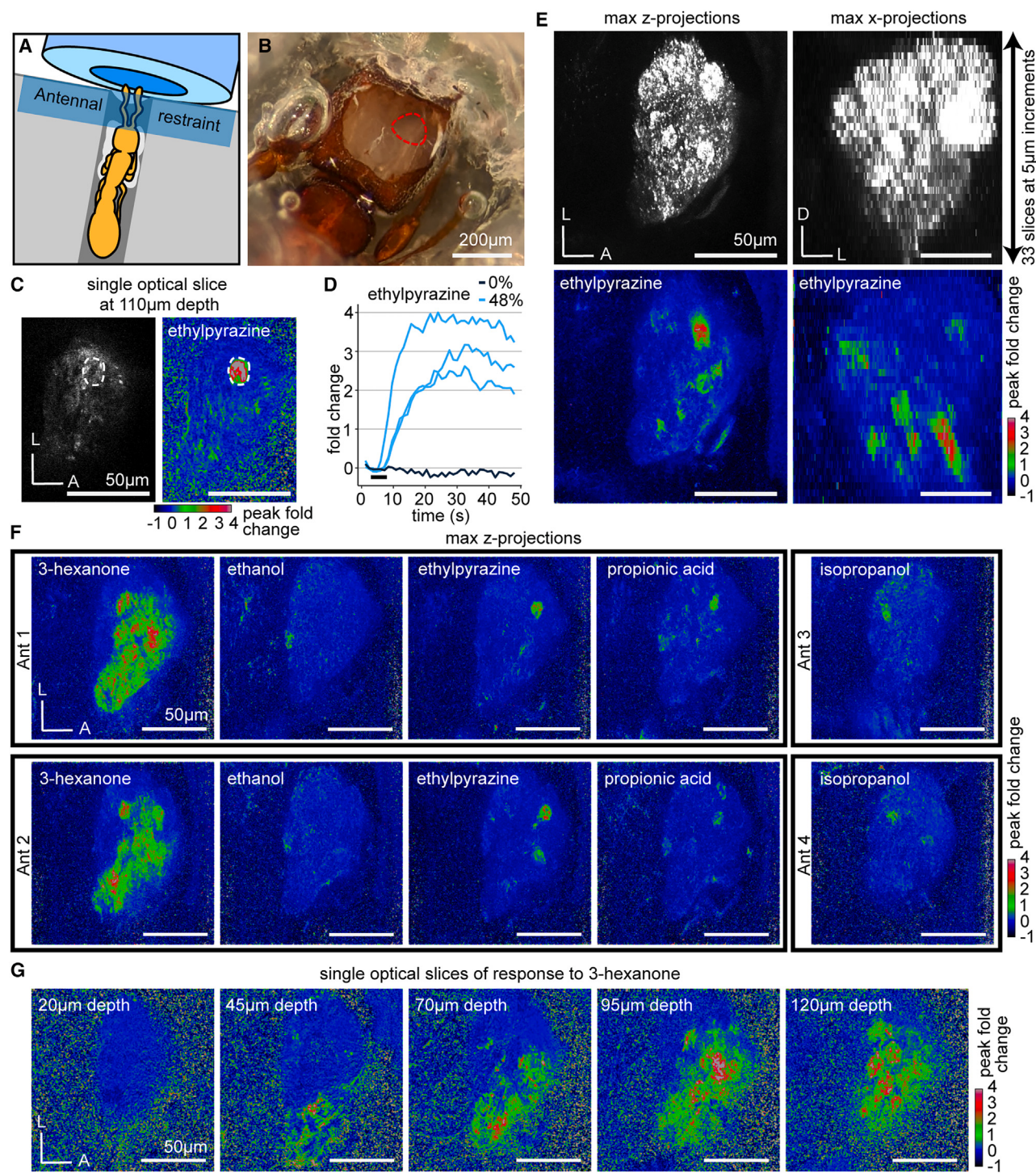


Figure 3. Imaging odor-evoked calcium responses in the antennal lobe

(A) Ant adhered to a plastic base with glue (white). A Parafilm strip restrains the antennae in front of the air tube.
(B) Cuticle and glandular tissue are removed to expose the AL (red outline).
(C) Single optical slice through the AL using two-photon microscopy showing raw fluorescence (left, brightness and contrast enhanced) and the peak fold change of fluorescence after a 5 s odor presentation at 48% concentration (right). A single glomerulus of interest is circled.
(D) Time series of calcium responses in the glomerulus from (C) from trials with ethylpyrazine or paraffin oil vehicle (0%); black bar indicates the 5 s odor presentation.

(legend continued on next page)

with time-correlated responses (Figure 3C). While previous studies of olfactory function in eusocial insects were limited to small subsets of ORs,^{71,72} a few olfactory sensilla^{73,74} or neurons,⁷⁵ or restricted subsections of the AL,^{25–34} our volumetric GCaMP-imaging approach allowed us to record from all olfactory glomeruli throughout the entire AL during single odor stimulus trials, without possible confounding signals from projection neurons, lateral interneurons, or glia, and without bias toward particular AL regions (Figure 3E).

To obtain a basic overview of odor representation, we presented ants ($n = 6$) with a panel of five general (non-pheromone) volatile odorants selected from the Database of Odorant Responses (DoOR) in *Drosophila*,³⁷ studies of OR function in other ants,⁷¹ and soil volatiles⁷⁶ (Table S3). To simplify the display of calcium responses while considering the entire AL, we calculated the peak fold change of fluorescence in each slice of the volumetric videos and then flattened them using max z-projection. Viewed this way, it was apparent that the ant AL exhibits properties of odor encoding that have been shown in other insects^{18,30}: each odorant activated a unique combination of glomeruli, and responses to the same odorant occurred in similar regions of the AL in different individuals, indicating that odor representation is qualitatively similar across individuals (Figure 3F). We also found that the breadth of glomerular responses varied dramatically across odorants, with most odorants activating a few glomeruli, whereas 3-hexanone activated large regions of the ventral/medial AL (Figures 3F and 3G). This demonstrates that our imaging approach can detect both sparse and broad calcium responses, if they occur.

Pheromone representation is sparse, and alarm-inducing compounds activate a single, shared glomerulus

To study the encoding of alarm pheromones, we first imaged responses to 4-methyl-3-hexanol in both ALs simultaneously ($n = 3$ ants) and found that response patterns were bilaterally symmetrical (Figure S4A). Given the equivalence between the two ALs, we then performed additional experiments imaging only the right AL. We presented each ant ($n = 13$ ants) with the four alarm pheromones at a range of concentrations (Figure 4A). Sparse, unique subsets of AL glomeruli responded to all pheromones, whereas the paraffin oil vehicle did not generate responses (Figures 4B and 4C). Fluorescence increases were frequently large (1- to 2-fold change) and lasted longer than the 5-s odor presentation. We did not observe any fluorescence decreases in response to odor, although we did detect small, non-specific decreases in fluorescence due to minor shifts in AL position and photobleaching. This artifact did not affect our ability to detect calcium responses, which remained robust after normalization for the duration of the experiment (Figures S4B and S4C). Comparison of calcium traces from two adjacent glomeruli showed high specificity of the response functions, without evidence for weak or transient calcium responses that might not be visible

from analysis of peak fold change (Figures S4B and S4C). The response patterns to the same alarm pheromone in different individuals were qualitatively similar, in accordance with what we observed for general odorants (Figures 3F and 4D).

We sought to determine how many of the ~500 glomeruli responded to each alarm pheromone by examining the max z-projections of the calcium responses. We identified all regions of interest corresponding to glomeruli activated in response to any of the four analyzed pheromones, quantified the mean peak fold change in response to each pheromone/concentration, and used a threshold of ≥ 0.2 mean peak fold change to find robust, odor-evoked responses (Figure S5A). Higher concentrations produced more robust responses, with a few more glomeruli passing the threshold, but overall spatial response patterns were similar across concentrations (Figures 4C, S4B, S4C, and S5A). Even at the highest concentration tested, the four pheromones activated a median of at most 6 glomeruli (Figure S5A). Despite the small number of responding glomeruli, we observed consistent partial overlap in the response patterns activated by the three compounds eliciting panic alarm responses, 4-methyl-3-heptanone, 4-methyl-3-heptanol, and 4-methyl-3-hexanol, with a single glomerulus activated by all three (Figure S5B). We refer to this glomerulus as the “panic glomerulus, broad” (PG_b). This finding is consistent with the expectation that these pheromones, which can elicit slightly different forms of alarm behavior,²² might share sensory pathways while also activating distinct sets of glomeruli. In contrast, although we sometimes observed responses to 6-methyl-5-hepten-2-one and either 4-methyl-3-heptanone or 4-methyl-3-hexanol in an overlapping region, those occurrences were rare and inconsistent (Figure S5C).

Alarm pheromone-responsive glomeruli are spatially stereotyped

To better understand the level of stereotypy in the ant AL, we decided to localize PG_b and characterize its local environment. The raw recordings revealed that PG_b is consistently located in the anterior part of the ventral AL hemi-lobe, adjacent to a gap containing no glomeruli (Figures 5A and 5B). This gap is distinct from the T7 glomerulus cluster, which is not reliably labeled by GCaMP6s. PG_b is located approximately halfway between the dorsal and ventral AL surfaces and is neighbored by two additional glomeruli that respond to alarm pheromones, with all three visible in the same optical plane (Figures 5A and 5B). While PG_b responds to 4-methyl-3-heptanone, 4-methyl-3-heptanol, and 4-methyl-3-hexanol, a nearby glomerulus responds to 6-methyl-5-hepten-2-one, which we refer to as the “6-methyl-5-hepten-2-one glomerulus” (6G). Both glomeruli were identified in 13/13 individuals. In 11/13 individuals, we identified a third neighboring glomerulus that responds to 4-methyl-3-heptanol and 4-methyl-3-hexanol, which we termed the “panic glomerulus, alcohol” (PG_a). Examination of the position of the three glomeruli in the z stacks and comparison with a previous

(E) Volumetric imaging of clonal raider ant ALs. Raw GCaMP6s fluorescence (top) in max z-projection (left) and max x-projection (right); responding glomeruli are visible throughout the volume (bottom) after presentation with ethylpyrazine (48%).

(F) Responses to general odorants in different individuals.

(G) Responses to 3-hexanone in five different optical slices. See Table S3 for vapor pressures of general odorants. D, dorsal; L, lateral; A, anterior.

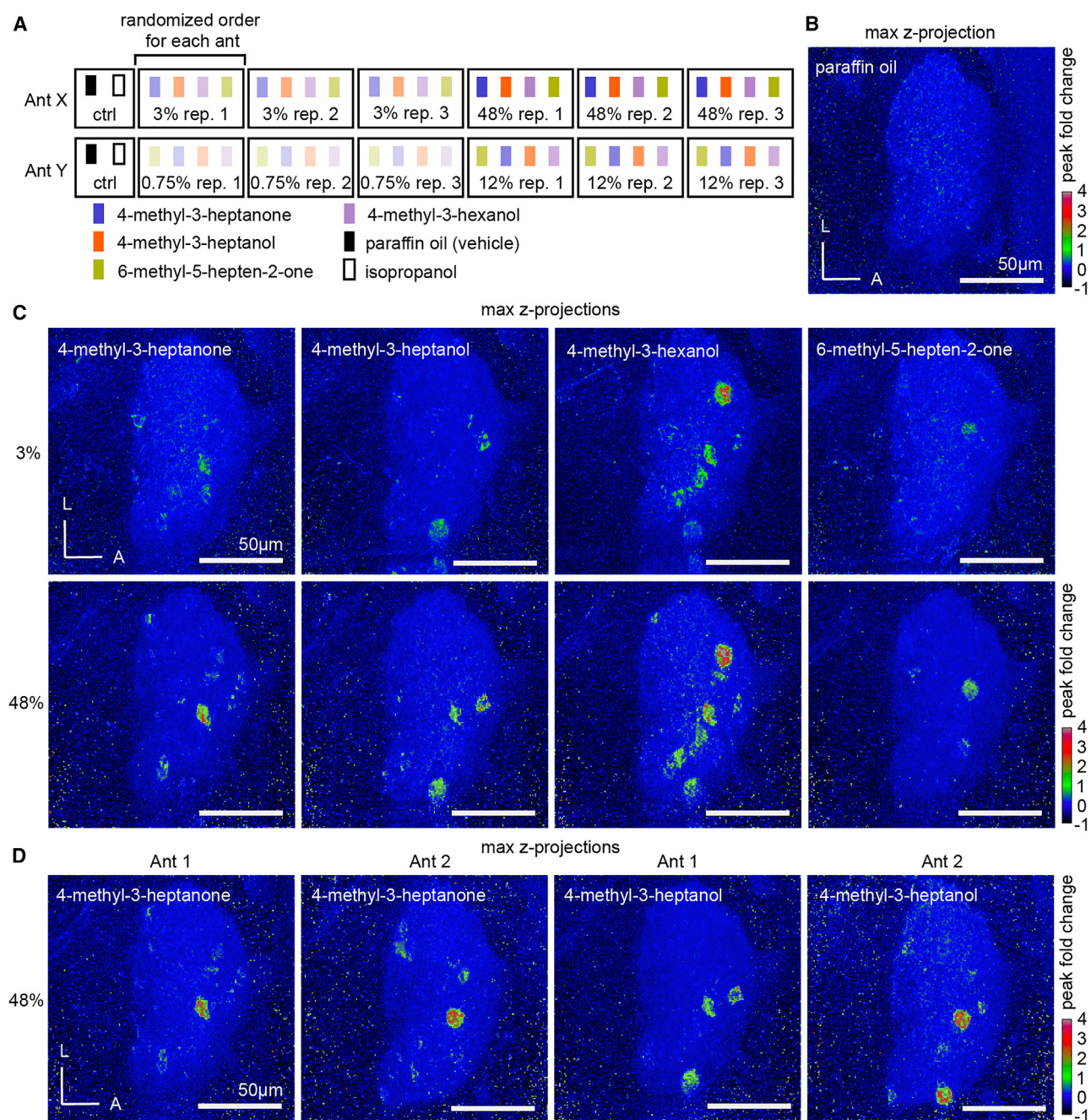


Figure 4. The representation of alarm pheromones in the antennal lobe

(A) Cartoon of the odor stimulus regime, with two ants shown as examples. Four alarm pheromone concentrations were tested in total (0.75%, 3.0%, 12.0%, and 48.0% v/v), but each individual ant was exposed to only two out of the four possible concentrations.

(B) The paraffin oil vehicle does not generate calcium responses.

(C) Representative max z-projections of peak fold changes from a single ant in response to four alarm pheromones at 3% and 48% concentrations.

(D) Two different individuals stimulated with 4-methyl-3-heptanone (left) and 4-methyl-3-heptanol (right) at high (48%) concentration. See Figure S4 for additional characterization of calcium responses. See Figure S5 for quantification of numbers of responding glomeruli. See Table S3 for vapor pressures of alarm pheromones. L, lateral; A, anterior.

segmentation of the AL⁹ showed that they are part of the T6 glomerulus cluster, which is innervated by OSNs from basiconic sensilla on the ventral surface of the ant antennal club that typi-

cally express members of the 9-exon OR subfamily (Figure 5B).⁹ In gross anatomy, PG_b, PG_a, and 6G resemble typical *O. biori* AL glomeruli and do not show obvious differences in shape or size.

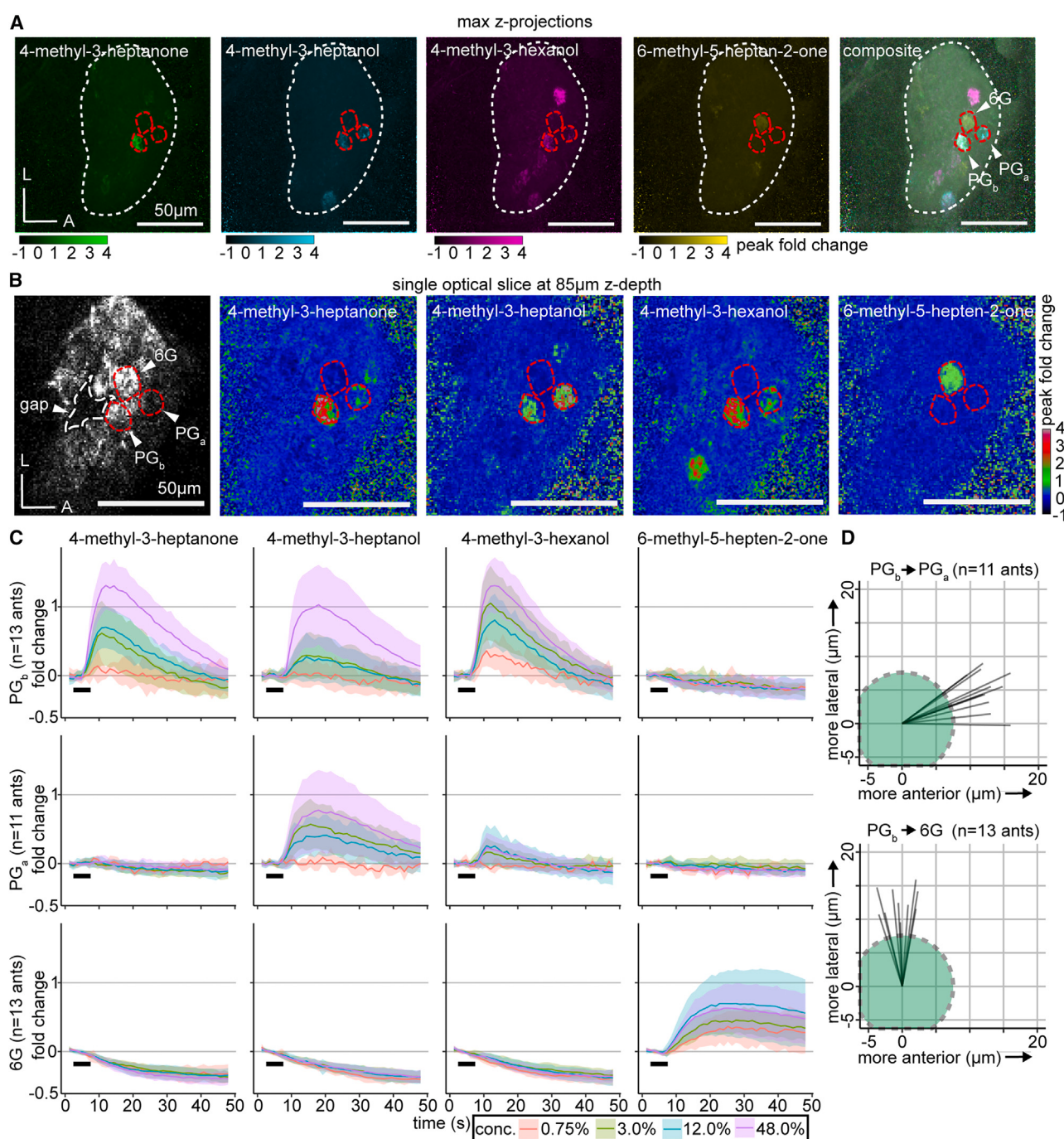


Figure 5. A glomerular cluster with stereotyped spatial organization and robust responses to alarm pheromones

(A) Whole-AL activation patterns for alarm pheromones overlap in several glomeruli. Three focal glomeruli are outlined in red.

(B) Single optical slice through the AL with the three focal glomeruli, which are adjacent to an AL region lacking glomeruli ("gap"; outlined in white). Fluorescence with enhanced brightness/contrast (left). Peak fold change in response to odors (right four panels). See [Figure S5](#) for quantifications of responding glomerulus numbers at different concentrations, and [Figure S6](#) for peak calcium response quantifications.

(C) Time series of calcium responses in PG_b (top), PG_a (middle), and 6G (bottom); mean \pm SD. Black bars indicate the 5 s odor presentation. See [Figure S7](#) for extended time series of responses to 6-methyl-5-hepten-2-one in 6G.

(D) Vectors of the spatial displacement between the centers of the PG_b and PG_a (top), and between the PG_b and 6G (bottom) glomeruli. Green circles represent a typical 15-µm-diameter glomerulus, for scale. L, lateral; A, anterior.

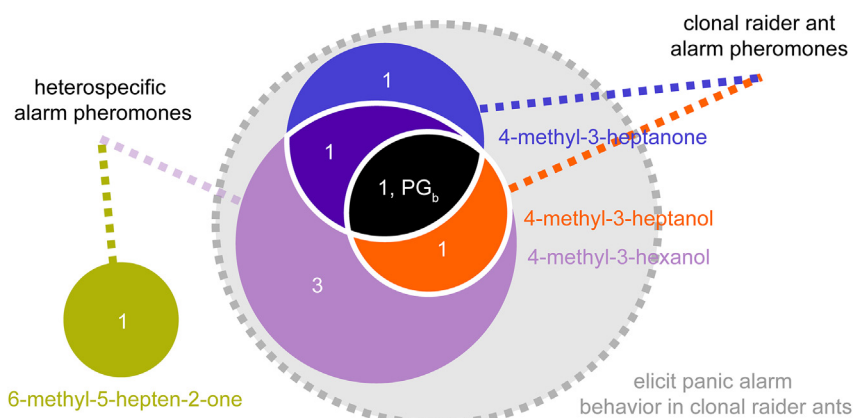


Figure 6. Conceptual schematic for the representation of alarm pheromones in the clonal raider ant AL

Numbers show the median number of responding glomeruli for each pheromone combination at the highest concentration tested (48%; n = 8 ants). PG_b is indicated on the diagram according to its response function.

To validate our initial finding that these three glomeruli are functionally distinct from one another, we aligned them across individuals and quantified glomerulus-specific odor responses. This demonstrated that, although PG_b, PG_a, and 6G are spatially adjacent, they each reliably respond to unique combinations of odorants, with several pheromone/glomerulus combinations producing no detectable responses (Figures 5C and S6). Importantly for its potential role in mediating alarm behavior, PG_b did not respond to 6-methyl-5-hepten-2-one, showing selectivity in its receptive tuning (Figures 5B, 5C, and S6).

Calcium responses had slow temporal dynamics, and in some cases, calcium signals remained elevated above baseline for the duration of a single 48-s recording trial. Examination of the temporal dynamics showed that, although responses in PG_b and PG_a peaked and then declined close to baseline by the end of the recording, responses in 6G were extremely slow, with a fluorescence plateau of tens of seconds (Figure 5C). We therefore performed additional odor presentations with 6-methyl-5-hepten-2-one with an extended recording period (144 s) and found that calcium responses did eventually return to baseline, although this sometimes took >100 s (Figure S7A). Quantifying time to response onset and time to response maximum for the different pheromones in the three focal glomeruli showed that different combinations had distinct temporal dynamics, as has been shown in other species (Figures S7B and S7C).^{35,36,77,78}

Our analyses thus far show that alarm pheromones evoke bilaterally symmetrical, qualitatively similar calcium responses across individuals and that the number of activated glomeruli is consistent for a given odor. However, they do not answer the question of whether the activated glomeruli are located in fixed positions within the AL as in *Drosophila* or whether there is significant local variation as in mice. To quantify the level of stereotypy, we examined the relative spatial positioning between PG_b, PG_a, and 6G along the medial-lateral and anterior-posterior axes (spatial resolution along the dorsal-ventral axis was insufficient for this analysis, especially given that these glomeruli are located at similar z-depths). We found that PG_a was always located anterior (mean distance between centers: 12.9 ± 1.9 SD μm), and slightly lateral (mean distance: 5.1 ± 2.9 SD μm) to PG_b (Figure 5D). In comparison, 6G was always lateral to PG_b (mean distance: 13.1 ± 2.6 SD μm), and in a similar position

along the anterior-posterior axis (mean distance: 0.6 ± 2.2 SD μm) (Figure 5D). The standard deviation values are much smaller than the typical diameter of a glomerulus ($10\text{--}20 \mu\text{m}$). We therefore conclude that these three glomeruli occupy stereotyped positions even within their

local glomerular cluster and show stereotyped odor response functions across individuals.

The median number and positions of responding glomeruli for each pheromone, in combination with the pheromones' behavioral outputs, allowed us to outline a conceptual schematic of alarm pheromone representation in the ant AL (Figure 6). The three pheromones with overlapping calcium response patterns all robustly elicited panic alarm behavior, whereas 6-methyl-5-hepten-2-one did not elicit panic alarm behavior and generated a non-overlapping response (Figure 6). These findings point to a shared pathway for eliciting panic alarm behavior, centered on PG_b.

DISCUSSION

In this study, we pioneered the combination of GCaMP with volumetric two-photon imaging to study social insect neurobiology. Because our stable transgenic line propagates clonally in the lab, these resources can be maintained indefinitely, adapted, and expanded to study many topics related to ant olfaction. To our knowledge, this has so far not been feasible in other eusocial insects due to challenges associated with transgenesis, performing crosses, and maintaining genetically modified strains. We used our transgenic line to address long-standing questions about pheromone representation in the ant AL. To study stereotypy in the ant olfactory system, we mapped a cluster of three AL glomeruli across individual clonal raider ants and found that they have consistent positions, spatial organization, and odor-evoked response functions. Ant ALs thus possess a high degree of spatial conservation at the scale of individual glomeruli, suggesting that, similar to *Drosophila*, axon targeting by OSNs can be stereotyped despite the vastly increased complexity of the olfactory system. However, additional work is required to determine whether this level of stereotypy is conserved across other parts of the AL.

The proportion of glomeruli that robustly responded to any alarm pheromone was very small, with a maximum of only 6 glomeruli displaying robust activation out of ~500 total. Contrary to previous studies on social insects,^{25–34} this sparse activation shows that alarm pheromones are in fact encoded by small numbers of glomeruli, similar to ecologically relevant chemicals in *Drosophila* and moths, such as sex pheromones^{79–83} and aversive

compounds including CO₂⁸⁴ and the microbial odorant geosmin.⁵⁶ This sparse encoding logic could simplify the neuronal computation required to respond to molecules indicative of danger, despite the complex olfactory environment of an ant colony.

With the exception of 3-hexanone, the general odorants tested here also only activated small numbers of glomeruli. Unlike in *Drosophila*,^{35–37} narrow glomerular tuning might thus be a more general property of the ant AL and could help compensate for the potentially much greater complexity of odor encoding implied by an expanded olfactory system. Using sparse encoding for sensory signals could decrease the probability of odor mixtures activating hundreds of glomeruli simultaneously, reducing the need for vast numbers of neural connections for decoding highly combinatorial signals. Sparse glomerular encoding could emerge from a simple organizational model where each glomerulus is innervated by a single OSN class that expresses a single narrowly tuned OR, and at least some ant ORs are indeed narrowly tuned.^{71,72} Alternatively, ant glomerular tuning properties could emerge from more complex patterns of OR expression or OSN connectivity, potentially via lateral inhibition^{85–87} or chemoreceptor co-expression.^{88,89} Collecting single-cell resolution data on OR expression and OSN connectivity in ants will be key for determining how ant olfactory coding properties arise. We also found that the temporal dynamics of calcium responses differed by odor and glomerulus. These features provide additional information that olfactory systems can use to interpret sensory inputs, including mixtures of odors.^{35,36,77,78}

Two of the alarm pheromones we studied are produced by the clonal raider ant, but we also investigated two additional alarm pheromones from other ant species. All four compounds share some structural features, including a methylated main carbon chain of six or seven carbons and alcohol or ketone functional groups. Of the two non-native compounds, 4-methyl-3-hexanol elicits panic alarm behavior and activates glomeruli that overlap with the two native alarm pheromones, 4-methyl-3-heptanone and 4-methyl-3-heptanol. This overlap can potentially be explained by the substantial structural similarity of these three compounds, including the similar arrangement of functional groups. It also suggests that the precise chemical structure of alarm pheromones could evolve rapidly across species, whereas the corresponding neural architecture underlying chemosensation and behavior is conserved.

A main difference between sex- and alarm pheromone detection systems is their level of specificity. Behavioral and neural responses to sex pheromones are highly specific, and close structural analogs elicit greatly reduced activity or even act as antagonists, a feature of the circuit logic that has been exploited in pest control.^{90,91} In contrast, compounds structurally similar to ant alarm pheromones usually elicit strong alarm responses, similar to the native pheromones.⁹² Our finding that some alarm pheromone-sensitive glomeruli respond to multiple panic-alarm-inducing compounds provides a neural mechanism for these behavioral observations, and shows that sex- and alarm pheromone detection systems can differ substantially in the chemical specificity of the pheromone-sensitive glomeruli. This difference could reflect the different selective pressures acting on these two systems. The high specificity of sex pheromones is a key contributor to prezygotic isolation in sympatric species.^{93,94} On

the other hand, in the case of alarm pheromones, a circuit logic similar to that of sex pheromone perception would open the door for predators and parasites to block alarm signaling within an ant colony using chemical antagonists or inhibitors. This could be catastrophic, leaving colonies defenseless against exploitation. The relatively broad excitability of the alarm pheromone detection system could thus confer protection against inhibitors. Although “appeasement allomones” have been described in ants, these chemicals are structurally unrelated and likely function through distinct sensory mechanisms from alarm pheromones.^{95–97} More often, rather than suppressing alarm signaling, ant predators and parasites manipulate their target species by inducing alarm responses,^{98,99–100} in some cases via pheromone mimicry.^{101,102}

In contrast to the other alarm pheromones, 6-methyl-5-hepten-2-one does not robustly cause panic alarm behavior in clonal raider ants. The glomerular response pattern is distinct from those of the panic-inducing alarm pheromones, which aligns with previous work, showing that compounds with different behavioral activity are usually detected through distinct olfactory channels.^{103,104} Interestingly, an ant-hunting spider uses 6-methyl-5-hepten-2-one to locate its prey, the meat ant *Iridomyrmex purpureus*.¹⁰⁵ Given that *O. biroi* is a specialized predator of other ants, our results raise the possibility that *O. biroi* may also employ alarm pheromones as cues to detect prey.

In both mice and *Drosophila*, olfactory glomeruli with similar chemical receptive ranges are clustered into functional subdomains, a pattern that can result from the duplication and gradual divergence of ancestral chemosensory receptors and their associated glomeruli.^{106–108} In our experiments, all four pheromones, which share structural similarities, activated combinations of spatially adjacent glomeruli. This suggests that the ant olfactory system also tends to map proximity in chemical space to actual spatial proximity in the AL. Here, we focused on glomeruli in the T6 cluster, which are mostly innervated by OSNs expressing ORs in the 9-exon subfamily.⁹ This subfamily is particularly highly expanded via gene duplications and undergoes rapid evolution in ants.^{9,10} Our results are thus consistent with a model in which recently duplicated ORs are not only activated by chemically related compounds but are expressed in OSNs innervating adjacent AL glomeruli. An electrophysiological study of subsets of randomly selected olfactory projection neurons in carpenter ants also found spatially clustered responses. However, these responses came from two chemically distinct alarm pheromone components, suggesting that spatial patterning in the ant AL may also reflect pheromone social functions in addition to chemical similarity.⁷⁵

Ant pheromone communication employs diverse chemical substrates, including compound mixtures.^{109,110} These mixtures can be complex, as is the case for the cuticular hydrocarbon blends that serve as nest membership gestalt odors.¹¹¹ Although ant ALs could in principle use broad encoding to represent such complex blends, insect olfactory systems can have an impressive capacity to reduce the complexity of ecologically relevant signal inputs. Mosquito ALs, for example, encode critical features of complex host odor mixtures using only a few glomeruli.⁵⁹ Future work should investigate whether the sparse encoding we report here for alarm pheromones holds true for nestmate recognition

cues and other types of pheromones used by ants. Indeed, previous studies in leaf-cutting ants suggested that a trail pheromone component may be detected primarily via a specialized macroglomerulus found only in large workers.^{44,112} This will help develop a general understanding of how glomerular tuning evolves in the context of chemical cues with high ecological relevance, complex chemical communication, and expanded olfactory systems.

Limitations of the study

We tested a relatively small panel of general odorants and alarm pheromones, and these compounds did not systematically span chemical space, limiting inferences about the general tuning properties of the ant olfactory system. General odorants with low vapor pressures generated no calcium responses at the tested concentrations, implying that different delivery methods will be required for these odorants.⁷² Furthermore, because it is generally challenging to determine the amount of odorant that an animal is exposed to and because our behavioral- and GCaMP-imaging experiments differed in many aspects of odorant delivery, we do not know whether the experienced amounts were comparable across the two assays. Similarly, we do not know what pheromone concentrations the animals encounter under naturalistic conditions, a common limitation that applies to the vast majority of pheromones. The general odorant and alarm pheromone imaging experiments were performed separately and in different individuals, preventing us from matching glomeruli between individuals across the two experiments or determining if the alarm pheromone-sensitive glomeruli also responded to general odorants. So far, we lack methods to functionally manipulate individual AL glomeruli in behaving ants and therefore cannot formally test whether specific glomeruli generate alarm behavior. These are all promising avenues for future studies of the ant olfactory system.

STAR★METHODS

Detailed methods are provided in the online version of this paper and include the following:

- [KEY RESOURCES TABLE](#)
- [RESOURCE AVAILABILITY](#)
 - Lead contact
 - Materials availability
 - Data and code availability
- [EXPERIMENTAL MODEL AND STUDY PARTICIPANT DETAILS](#)
 - Ant husbandry and maintenance
- [METHOD DETAILS](#)
 - Behavior
 - Generation of transgenic ants
 - Phenotyping transgenic ants
 - *In vivo* calcium imaging
- [QUANTIFICATION AND STATISTICAL ANALYSIS](#)

SUPPLEMENTAL INFORMATION

Supplemental information can be found online at <https://doi.org/10.1016/j.cell.2023.05.025>.

ACKNOWLEDGMENTS

We thank members of the Kronauer, Ruta, and Vosshall labs at Rockefeller University for helpful advice and discussions. Ben Matthews provided samples of the hyPBase^{apis}, pBAC-ECFP-15xQUAS_TATA-SV40, and pBac-dsRed-ORCO_9kbProm-QF2 plasmids. We thank Martin Beye for permission to use the hyPBase^{apis} plasmid and Chris Potter for permission to use the pBAC-ECFP-15xQUAS_TATA-SV40 and pBac-dsRed-ORCO_9kbProm-QF2 plasmids prior to their appearance in publications. We thank Rob Harrell for sharing an alternate [ie1-dsRed] plasmid that was used in test injections. The anti-SYNORF1 antibody developed by E. Buchner was obtained from the Developmental Studies Hybridoma Bank, created by the NICHD of the NIH and maintained at the University of Iowa, Department of Biology. We thank Meg Younger for initial training and access to a two-photon microscope. We thank Daniel Pastor for sharing his protocol for immunohistochemistry in the whole-mounted antennal club. DNA sequencing was performed at the Rockefeller University Genomics Resource Center. Some confocal microscopy was performed at the Rockefeller University Bio-Imaging Resource Center. This work was supported by the National Institute of General Medical Sciences of the National Institutes of Health under award number R35GM127007, as well as the National Institute of Neurological Disorders and Stroke under award number R01NS123899 to D.J.C.K. The content is solely the responsibility of the authors and does not necessarily represent the official views of the National Institutes of Health. Additional support was provided by a Faculty Scholars Award from the Howard Hughes Medical Institute to D.J.C.K. T.H. was supported by an NSF Graduate Research Fellowship under award number 1946429 and a project grant from the Kavli Neural Systems Institute at The Rockefeller University. D.D.F. is an Open Philanthropy Fellow of the Life Sciences Research Foundation. L.E.L. was supported by an NSF Graduate Research Fellowship under award number DGE 194642. This work was supported in part by a grant to The Rockefeller University from the Howard Hughes Medical Institute through the James H. Gilliam Fellowships for Advanced Study program (to L.E.L. and D.J.C.K.). D.J.C.K. is an investigator of the Howard Hughes Medical Institute. This is Clonal Raider Ant Project paper number 28.

AUTHOR CONTRIBUTIONS

T.H., W.T., L.O.-C., and D.J.C.K. designed the transgenics experiments. L.O.-C., S.V.-R., A.R., and T.H. maintained and reared ant colonies and collected eggs for injections. T.H. cloned the transgene constructs and performed the injections. L.E.L. performed and analyzed the behavioral experiments. D.D.F. performed the immunohistochemistry and confocal imaging and built the olfactometer. T.H. performed the epifluorescence imaging and AL reconstructions. K.D.L. prepared libraries for sequencing and performed the genomic analyses. T.H., D.D.F., and D.J.C.K. designed the functional imaging experiments. T.H. performed and analyzed the functional imaging experiments. T.H. and D.J.C.K. wrote the paper, and all authors read, edited, and approved the manuscript for publication. D.J.C.K. supervised the project.

DECLARATION OF INTERESTS

The authors declare no competing interests.

Received: December 28, 2022

Revised: March 30, 2023

Accepted: May 16, 2023

Published: June 14, 2023

REFERENCES

1. Strausfeld, N.J., and Hildebrand, J.G. (1999). Olfactory systems: common design, uncommon origins? *Curr. Opin. Neurobiol.* 9, 634–639. [https://doi.org/10.1016/S0959-4388\(99\)00019-7](https://doi.org/10.1016/S0959-4388(99)00019-7).

2. Vosshall, L.B., Wong, A.M., and Axel, R. (2000). An olfactory sensory map in the fly brain. *Cell* 102, 147–159. [https://doi.org/10.1016/S0092-8674\(00\)00021-0](https://doi.org/10.1016/S0092-8674(00)00021-0).
3. Zhao, Z., and McBride, C.S. (2020). Evolution of olfactory circuits in insects. *J. Comp. Physiol. A Neuroethol. Sens. Neural Behav. Physiol.* 206, 353–367. <https://doi.org/10.1007/s00359-020-01399-6>.
4. Mysore, K., Subramanian, K.A., Sarasij, R.C., Suresh, A., Shyamala, B.V., VijayRaghavan, K., and Rodrigues, V. (2009). Caste and sex specific olfactory glomerular organization and brain architecture in two sympatric ant species *Camponotus sericeus* and *Camponotus compressus* (Fabricius, 1798). *Arthropod Struct. Dev.* 38, 485–497. <https://doi.org/10.1016/j.asd.2009.06.001>.
5. Kelber, C., Rössler, W., and Kleineidam, C.J. (2010). Phenotypic plasticity in number of glomeruli and sensory innervation of the antennal lobe in leaf-cutting ant workers (*A. vollenweideri*). *Dev. Neurobiol.* 70, 222–234. <https://doi.org/10.1002/dneu.20782>.
6. Smith, C.D., Zimin, A., Holt, C., Abouheif, E., Benton, R., Cash, E., Croset, V., Currie, C.R., Elhaik, E., Elsik, C.G., et al. (2011). Draft genome of the globally widespread and invasive Argentine ant (*Linepithema humile*). *Proc. Natl. Acad. Sci. USA* 108, 5673–5678. <https://doi.org/10.1073/pnas.1008617108>.
7. Zhou, X., Slone, J.D., Rokas, A., Berger, S.L., Liebig, J., Ray, A., Reinberg, D., and Zwiebel, L.J. (2012). Phylogenetic and transcriptomic analyses of chemosensory receptors in a pair of divergent ant species reveals sex-specific signatures of odor coding. *PLoS Genet.* 8, e1002930. <https://doi.org/10.1371/journal.pgen.1002930>.
8. Zhou, X., Rokas, A., Berger, S.L., Liebig, J., Ray, A., and Zwiebel, L.J. (2015). Chemoreceptor evolution in Hymenoptera and its implications for the evolution of eusociality. *Genome Biol. Evol.* 10, 2490–2500. <https://doi.org/10.1093/gbe/evy131>.
9. McKenzie, S.K., Fetter-Pruneda, I., Ruta, V., and Kronauer, D.J.C. (2016). Transcriptomics and neuroanatomy of the clonal raider ant implicate an expanded clade of odorant receptors in chemical communication. *Proc. Natl. Acad. Sci. USA* 113, 14091–14096. <https://doi.org/10.1073/pnas.1610800113>.
10. McKenzie, S.K., and Kronauer, D.J.C. (2018). The genomic architecture and molecular evolution of ant odorant receptors. *Genome Res.* 28, 1757–1765. <https://doi.org/10.1101/gr.237123.118>.
11. Ryba, A.R., McKenzie, S.K., Olivos-Cisneros, L., Clowney, E.J., Pires, P.M., and Kronauer, D.J.C. (2020). Comparative development of the ant chemosensory system. *Curr. Biol.* 30, 3223–3230.e4. <https://doi.org/10.1016/j.cub.2020.05.072>.
12. Trible, W., Olivos-Cisneros, L., Saragosti, J., Chang, S.K., Matthews, B.J., Oxley, P.R., and Kronauer, D.J.C. (2017). orco mutagenesis causes loss of antennal lobe glomeruli and impaired social behavior in ants. *Cell* 170, 727–735. <https://doi.org/10.1016/j.cell.2017.07.001>.
13. Ferguson, S.T., Bakis, I., and Zwiebel, L.J. (2021). Advances in the study of olfaction in eusocial ants. *Insects* 12, 252. <https://doi.org/10.3390/insects12030252>.
14. Benton, R. (2022). *Drosophila* olfaction: past, present, and future. *Proc. R. Soc. Lond. B* 289, 202202054. <https://doi.org/10.1098/rspb.2022.2054>.
15. Gao, Q., Yuan, B., and Chess, A. (2000). Convergent projections of *Drosophila* olfactory neurons to specific glomeruli in the antennal lobe. *Nat. Neurosci.* 3, 780–785. <https://doi.org/10.1038/77680>.
16. Stocker, R.F. (1994). The organization of the chemosensory system in *Drosophila melanogaster*: a review. *Cell Tissue Res.* 275, 3–26. <https://doi.org/10.1007/BF00305372>.
17. Stocker, R.F., Lienhard, M.C., Borst, A., and Fischbach, K.F. (1990). Neuronal architecture of the antennal lobe in *Drosophila melanogaster*. *Cell Tissue Res.* 262, 9–34. <https://doi.org/10.1007/BF00327741>.
18. Wang, J.W., Wong, A.M., Flores, J., Vosshall, L.B., and Axel, R. (2003). Two-photon calcium imaging reveals an odor-evoked map of activity in the fly brain. *Cell* 112, 271–282. [https://doi.org/10.1016/S0092-8674\(03\)00004-7](https://doi.org/10.1016/S0092-8674(03)00004-7).
19. Duffield, R.M., Blum, M.S., and Wheeler, J.M. (1976). Alkylpyrazine alarm pheromones in primitive ants with small colonial units. *Comp. Biochem. Physiol.* 54, 439–440. [https://doi.org/10.1016/0305-0491\(76\)90116-4](https://doi.org/10.1016/0305-0491(76)90116-4).
20. Wilson, E.O., and Regnier, F.E.J. (1971). The evolution of the alarm-defense system in the formicine ants. *Am. Nat.* 105, 279–289. <https://doi.org/10.1086/282724>.
21. Smith, A.A., and Haight, K.L. (2008). Army ants as research and collection tools. *J. Insect Sci.* 8, 1–5. <https://doi.org/10.1673/031.008.7101>.
22. Lopes, L.E., Frank, E.T., Kárpáti, Z., Schmitt, T., and Kronauer, D.J.C. (2023). The alarm pheromone and alarm response of the clonal raider ant. *J. Chem. Ecol.* 49, 1–10. <https://doi.org/10.1007/s10886-023-01407-4>.
23. Blum, M.S. (1969). Alarm pheromones. *Annu. Rev. Entomol.* 14, 57–80. <https://doi.org/10.1146/annurev.en.14.010169.000421>.
24. Vander Meer, R.K., and Alonso, L.E. (1998). Pheromone directed behavior in ants. In *Pheromone Communication in Social Insects*, R.K. Vander Meer, M.D. Breed, K.E. Espelie, and M. Winston, eds. (Westview Press), pp. 159–192.
25. Galizia, C.G., Menzel, R., and Hölldobler, B. (1999). Optical imaging of odor-evoked glomerular activity patterns in the antennal lobes of the ant *Camponotus rufipes*. *Naturwissenschaften* 86, 533–537. <https://doi.org/10.1007/s001140050069>.
26. Zube, C., Kleineidam, C.J., Kirschner, S., Neef, J., and Rössler, W. (2008). Organization of the olfactory pathway and odor processing in the antennal lobe of the ant *Camponotus floridanus*. *J. Comp. Neurol.* 506, 425–441. <https://doi.org/10.1002/cne.21548>.
27. Brandstaetter, A.S., Rössler, W., and Kleineidam, C.J. (2011). Friends and foes from an ant brain's point of view – neuronal correlates of colony odors in a social insect. *PLoS One* 6, e21383. <https://doi.org/10.1371/journal.pone.0021383>.
28. Joerges, J., Küttnér, A., Galizia, C.G., and Menzel, R. (1997). Representations of odours and odour mixtures visualized in the honeybee brain. *Nature* 387, 285–288. <https://doi.org/10.1038/387285a0>.
29. Galizia, C.G., Nägler, K., Hölldobler, B., and Menzel, R. (1998). Odour coding is bilaterally symmetrical in the antennal lobes of honeybees (*Apis mellifera*). *Eur. J. Neurosci.* 10, 2964–2974. <https://doi.org/10.1111/j.1460-9568.1998.00303.x>.
30. Sachse, S., Rappert, A., and Galizia, C.G. (1999). The spatial representation of chemical structures in the antennal lobe of honeybees: steps towards the olfactory code. *Eur. J. Neurosci.* 11, 3970–3982. <https://doi.org/10.1046/j.1460-9568.1999.00826.x>.
31. Guerrieri, F., Schubert, M., Sandoz, J.C., and Giurfa, M. (2005). Perceptual and neural olfactory similarity in honeybees. *PLoS Biol.* 3, e60. <https://doi.org/10.1371/journal.pbio.0030060>.
32. Carcaud, J., Giurfa, M., and Sandoz, J.-C. (2015). Differential combinatorial coding of pheromones in two olfactory subsystems of the honey bee brain. *J. Neurosci.* 35, 4157–4167. <https://doi.org/10.1523/JNEUROSCI.0734-14.2015>.
33. Paoli, M., and Galizia, G.C. (2021). Olfactory coding in honeybees. *Cell Tissue Res.* 383, 35–58. <https://doi.org/10.1007/s00441-020-03385-5>.
34. Haase, A., Rigosi, E., Trona, F., Anfora, G., Vallortigara, G., Antolini, R., and Vinegoni, C. (2010). In-vivo two-photon imaging of the honey bee antennal lobe. *Biomed. Opt. Express* 2, 131–138. <https://doi.org/10.1364/BOE.1.000131>.
35. Laurent, G. (1999). A systems perspective on early olfactory coding. *Science* 286, 723–728. <https://doi.org/10.1126/science.286.5440.723>.
36. Hallen, E.A., and Carlson, J.R. (2006). Coding of odors by a receptor repertoire. *Cell* 125, 143–160. <https://doi.org/10.1016/j.cell.2006.01.050>.
37. Münch, D., and Galizia, C.G. (2016). DoOR 2.0 - Comprehensive mapping of *Drosophila melanogaster* odorant responses. *Sci. Rep.* 6, 21841. <https://doi.org/10.1038/srep21841>.

38. Yan, H., Opachaloemphan, C., Mancini, G., Yang, H., Gallitto, M., Mleinck, J., Leibholz, A., Haight, K., Ghaninia, M., Huo, L., et al. (2017). An engineered *orco* mutation in ants produces aberrant social behavior and defective neural development. *Cell* 170, 736–747.e9. <https://doi.org/10.1016/j.cell.2017.06.051>.
39. Duan, Q., and Volkan, P.C. (2020). Ant olfaction: smells like an insect, develops like a mammal. *Curr. Biol.* 30, R950–R952. <https://doi.org/10.1016/j.cub.2020.06.074>.
40. Lodovichi, C., and Belluscio, L. (2012). Odorant receptors in the formation of the olfactory bulb circuitry. *Physiology* 27, 200–212. <https://doi.org/10.1152/physiol.00015.2012>.
41. Schaefer, M.L., Finger, T.E., and Restrepo, D. (2001). Variability of position of the P2 glomerulus within a map of the mouse olfactory bulb. *J. Comp. Neurol.* 436, 351–362. <https://doi.org/10.1002/cne.1072>.
42. Strotmann, J., Conzelmann, S., Beck, A., Feinstein, P., Breer, H., and Mombaerts, P. (2000). Local permutations in the glomerular array of the mouse olfactory bulb. *J. Neurosci.* 20, 6927–6938. <https://doi.org/10.1523/JNEUROSCI.20-18-06927.2000>.
43. Zapiec, B., and Mombaerts, P. (2015). Multiplex assessment of the positions of odorant receptor-specific glomeruli in the mouse olfactory bulb by serial two-photon tomography. *Proc. Natl. Acad. Sci. USA* 112, E5873–E5882. <https://doi.org/10.1073/pnas.1512135112>.
44. Kuebler, L.S., Kelber, C., and Kleineidam, C.J. (2010). Distinct antennal lobe phenotypes in the leaf-cutting ant (*Atta vollenweideri*). *J. Comp. Neurol.* 518, 352–365. <https://doi.org/10.1002/cne.22217>.
45. Oxley, P.R., Ji, L., Fetter-Pruneda, I., McKenzie, S.K., Li, C., Hu, H., Zhang, G., and Kronauer, D.J.C. (2014). The genome of the clonal raider ant *Cerapachys biroi*. *Curr. Biol.* 24, 451–458. <https://doi.org/10.1016/j.cub.2014.01.018>.
46. Chandra, V., Gal, A., and Kronauer, D.J.C. (2021). Colony expansions underlie the evolution of army ant mass raiding. *Proc. Natl. Acad. Sci. USA* 118, e2026534118. <https://doi.org/10.1073/pnas.2026534118>.
47. Bernardi, R., Cardani, C., Ghiringhelli, D., Selva, A., Baggini, A., and Pavan, M. (1967). On the components of secretion of mandibular glands of the ant. *Tetrahedron Lett.* 8, 3893–3896. [https://doi.org/10.1016/S0040-4039\(01\)89747-1](https://doi.org/10.1016/S0040-4039(01)89747-1).
48. Duffield, R.M., Brand, J.M., and Blum, M.S. (1977). 6-methyl-5-hepten-2-one in *Formica* species: identification and function as an alarm pheromone (Hymenoptera: Formicidae). *Ann. Entomol. Soc. Am.* 70, 309–310. <https://doi.org/10.1093/aesa/70.3.309>.
49. Han, S., Chen, W., and Elgar, M.A. (2022). An ambiguous function of an alarm pheromone in the collective displays of the Australian meat ant, *Iridomyrmex purpureus*. *Ethology* 128, 70–76. <https://doi.org/10.1111/eth.13241>.
50. Keegans, S.J., Billen, J., Morgan, E.D., and Gökcen, O.A. (1993). Volatile glandular secretions of three species of new world army ants, *Eciton burchelli*, *Labidus coecus*, and *Labidus praedator*. *J. Chem. Ecol.* 19, 2705–2719. <https://doi.org/10.1007/BF00980702>.
51. McGurk, D.J. (1968). I. Studies of volatile compounds from ants II. Degradation studies and structure proof of cis, cis-nepetalactone (Oklahoma State University).
52. Morgan, E.D., Jackson, B.D., Keegans, S.J., Nicholls, D.J., Ali, M.F., and Cammaerts, R. (1992). Alkanols in the mandibular gland secretion of the ant *Tetramorium caespitum*. *Belg. J. Zool.* 122, 69–74.
53. Oldham, N.J., Morgan, E.D., Gobin, B., Schoeters, E., and Billen, J. (1994). Volatile secretions of the old world army ant *Aenictus rotundatus* and chemotaxonomic implications of army ant Dufour gland chemistry. *J. Chem. Ecol.* 20, 3297–3305. <https://doi.org/10.1007/BF02033727>.
54. Pasteels, J.M., Verhaeghe, J.C., Braekman, J.C., Daloz, D., and Tursch, B. (1980). Caste-dependent pheromones in the head of the ant *Tetramorium caespitum*. *J. Chem. Ecol.* 6, 467–472. <https://doi.org/10.1007/BF01402923>.
55. Pasteels, J.M., Verhaeghe, J.C., Ottinger, R., Braekman, J.C., and Daloz, D. (1981). Absolute configuration of (3R,4S)-4-methyl-3-hexanol - A pheromone from the head of the ant *Tetramorium impurum* Foerster. *Insect Biochem.* 11, 675–678. [https://doi.org/10.1016/0020-1790\(81\)90057-3](https://doi.org/10.1016/0020-1790(81)90057-3).
56. Stensmyr, M.C., Dweck, H.K.M., Farhan, A., Ibba, I., Strutz, A., Mukunda, L., Linz, J., Grabe, V., Steck, K., Lavista-Llanos, S., et al. (2012). A conserved dedicated olfactory circuit for detecting harmful microbes in *Drosophila*. *Cell* 151, 1345–1357. <https://doi.org/10.1016/j.cell.2012.09.046>.
57. Carcaud, J., Otte, M., Grünwald, B., Haase, A., Sandoz, J.C., and Beye, M. (2023). Multisite imaging of neural activity using a genetically encoded calcium indicator in the honey bee. *PLoS Biol.* 21, e3001984. <https://doi.org/10.1371/journal.pbio.3001984>.
58. Stökl, J., Strutz, A., Dafni, A., Svatos, A., Doubsky, J., Knaden, M., Sachse, S., Hansson, B.S., and Stensmyr, M.C. (2010). A deceptive pollination system targeting drosophilids through olfactory mimicry of yeast. *Curr. Biol.* 20, 1846–1852. <https://doi.org/10.1016/j.cub.2010.09.033>.
59. Zhao, Z., Zung, J.L., Hinze, A., Kriete, A.L., Iqbal, A., Younger, M.A., Matthews, B.J., Merhof, D., Thibierge, S., Igneil, R., et al. (2022). Mosquito brains encode unique features of human odour to drive host seeking. *Nature* 605, 706–712. <https://doi.org/10.1038/s41586-022-04675-4>.
60. Chen, T.W., Wardill, T.J., Sun, Y., Pulver, S.R., Renninger, S.L., Baohan, A., Schreiter, E.R., Kerr, R.A., Orger, M.B., Jayaraman, V., et al. (2013). Ultrasensitive fluorescent proteins for imaging neuronal activity. *Nature* 499, 295–300. <https://doi.org/10.1038/nature12354>.
61. Riabinina, O., Luginbuhl, D., Marr, E., Liu, S., Wu, M.N., Luo, L., and Potter, C.J. (2015). Improved and expanded Q-system reagents for genetic manipulations. *Nat. Methods* 12, 37–54. <https://doi.org/10.1038/nmeth.3250>.
62. Anderson, M.A.E., Gross, T.L., Myles, K.M., and Adelman, Z.N. (2010). Validation of novel promoter sequences derived from two endogenous ubiquitin genes in transgenic *Aedes aegypti*. *Insect Mol. Biol.* 19, 441–449. <https://doi.org/10.1111/j.1365-2583.2010.01005.x>.
63. Suzuki, M.G., Funaguma, S., Kanda, T., Tamura, T., and Shimada, T. (2003). Analysis of the biological functions of a doublesex homologue in *Bombyx mori*. *Dev. Genes Evol.* 213, 345–354. <https://doi.org/10.1007/s00427-003-0334-8>.
64. Masumoto, M., Ohde, T., Shiomi, K., Yaginuma, T., and Niimi, T. (2012). A baculovirus immediate-early gene, *ie1*, promoter drives efficient expression of a transgene in both *Drosophila melanogaster* and *Bombyx mori*. *PLoS One* 7, e49323. <https://doi.org/10.1371/journal.pone.0049323>.
65. Otte, M., Netschitailo, O., Kaftanoglu, O., Wang, Y., Page, R.E., Jr., and Beye, M. (2018). Improving genetic transformation rates in honeybees. *Sci. Rep.* 8, 16534. <https://doi.org/10.1038/s41598-018-34724-w>.
66. Habenstein, J., Amini, E., Grübel, K., el Jundi, B., and Rössler, W. (2020). The brain of *Cataglyphis* ants: neuronal organization and visual projections. *J. Comp. Neurol.* 528, 3479–3506. <https://doi.org/10.1002/cne.24934>.
67. Ferkey, D.M., Hyde, R., Haspel, G., Dionne, H.M., Hess, H.A., Suzuki, H., Schafer, W.R., Koelle, M.R., and Hart, A.C. (2007). *C. elegans* G protein regulator RGS-3 controls sensitivity to sensory stimuli. *Neuron* 53, 39–52. <https://doi.org/10.1016/j.neuron.2006.11.015>.
68. Tian, L., Hires, S.A., and Looger, L.L. (2012). Imaging neuronal activity with genetically encoded calcium indicators. *Cold Spring Harb. Protoc.* 2012, 647–656. <https://doi.org/10.1101/pdb.top069609>.
69. Bellen, H.J., Lewis, R.W., He, Y., Carlson, J.W., Evans-Holm, M., Bae, E., Kim, J., Metaxakis, A., Savakis, C., Schulze, K.L., et al. (2011). The *Drosophila* gene disruption project: progress using transposons with distinctive site specificities. *Genetics* 188, 731–743. <https://doi.org/10.1534/genetics.111.126995>.
70. Galizia, C.G., Joerges, J., Küttner, A., Faber, T., and Menzel, R. (1997). A semi-in-vivo preparation for optical recording of the insect brain.

- J. Neurosci. Methods 76, 61–69. [https://doi.org/10.1016/S0165-0270\(97\)00080-0](https://doi.org/10.1016/S0165-0270(97)00080-0).
71. Slone, J.D., Pask, G.M., Ferguson, S.T., Millar, J.G., Berger, S.L., Reinberg, D., Liebig, J., Ray, A., and Zwiebel, L.J. (2017). Functional characterization of odorant receptors in the ponerine ant, *Harpegnathos saltator*. Proc. Natl. Acad. Sci. USA 114, 8586–8591. <https://doi.org/10.1073/pnas.1704647114>.
72. Pask, G.M., Slone, J.D., Millar, J.G., Das, P., Moreira, J.A., Zhou, X., Bello, J., Berger, S.L., Bonasio, R., Desplan, C., et al. (2017). Specialized odorant receptors in social insects that detect cuticular hydrocarbon cues and candidate pheromones. Nat. Commun. 8, 297. <https://doi.org/10.1038/s41467-017-00099-1>.
73. Ozaki, M., Wada-Katsumata, A., Fujikawa, K., Iwasaki, M., Yokohari, F., Satoji, Y., Nisimura, T., and Yamaoka, R. (2005). Ant nestmate and non-nestmate discrimination by a chemosensory sensillum. Science 309, 311–314. <https://doi.org/10.1126/science.1105244>.
74. Sharma, K.R., Enzmann, B.L., Schmidt, Y., Moore, D., Jones, G.R., Parker, J., Berger, S.L., Reinberg, D., Zwiebel, L.J., Breit, B., et al. (2015). Cuticular hydrocarbon pheromones for social behavior and their coding in the ant antenna. Cell Rep. 12, 1261–1271. <https://doi.org/10.1016/j.celrep.2015.07.031>.
75. Yamagata, N., Nishino, H., and Mizunami, M. (2006). Pheromone-sensitive glomeruli in the primary olfactory centre of ants. Proc. R. Soc. Lond. B 273, 2219–2225. <https://doi.org/10.1098/rspb.2006.3565>.
76. Insam, H., and Seewald, M.S.A. (2010). Volatile organic compounds (VOCs) in soils. Biol. Fertil. Soils 46, 199–213. <https://doi.org/10.1007/s00374-010-0442-3>.
77. Hallen, E.A., Ho, M.G., and Carlson, J.R. (2004). The molecular basis of odor coding in the *Drosophila* antenna. Cell 117, 965–979. <https://doi.org/10.1016/j.cell.2004.05.012>.
78. Su, C.Y., Martelli, C., Emonet, T., and Carlson, J.R. (2011). Temporal coding of odor mixtures in an olfactory receptor neuron. Proc. Natl. Acad. Sci. USA 108, 5075–5080. <https://doi.org/10.1073/pnas.1100369108>.
79. Kurtovic, A., Widmer, A., and Dickson, B.J. (2007). A single class of olfactory neurons mediates behavioral responses to a *Drosophila* sex pheromone. Nature 446, 542–546. <https://doi.org/10.1038/nature05672>.
80. Christensen, T.A., and Hildebrand, J.G. (1987). Male-specific, sex pheromone-selective projection neurons in the antennal lobes of the moth *Manduca sexta*. J. Comp. Physiol. A 160, 553–569. <https://doi.org/10.1007/BF00611929>.
81. Sakurai, T., Nakagawa, T., Mitsuno, H., Mori, H., Endo, Y., Tanoue, S., Yasukochi, Y., Touhara, K., and Nishioka, T. (2004). Identification and functional characterization of a sex pheromone receptor in the silkworm *Bombyx mori*. Proc. Natl. Acad. Sci. USA 101, 16653–16658. <https://doi.org/10.1073/pnas.0407596101>.
82. Hildebrand, J.G., and Shepherd, G.M. (1997). Mechanisms of olfactory discrimination: converging evidence for common principles across phyla. Annu. Rev. Neurosci. 20, 595–631. <https://doi.org/10.1146/annurev.neuro.20.1.595>.
83. Dweck, H.K.M., Ebrahim, S.A.M., Thoma, M., Mohamed, A.A.M., Keesey, I.W., Trona, F., Lavista-Llanos, S., Svatos, A., Sachse, S., Knaden, M., et al. (2015). Pheromones mediating copulation and attraction in *Drosophila*. Proc. Natl. Acad. Sci. USA 112, E2829–E2835. <https://doi.org/10.1073/pnas.1504527112>.
84. Jones, W.D., Cayirlioglu, P., Kadov, I.G., and Vosshall, L.B. (2007). Two chemosensory receptors together mediate carbon dioxide detection in *Drosophila*. Nature 445, 86–90. <https://doi.org/10.1038/nature05466>.
85. Su, C.Y., Menuz, K., Reisert, J., and Carlson, J.R. (2012). Non-synaptic inhibition between grouped neurons in an olfactory circuit. Nature 492, 66–71. <https://doi.org/10.1038/nature11712>.
86. Root, C.M., Masuyama, K., Green, D.S., Enell, L.E., Nässel, D.R., Lee, C.H., and Wang, J.W. (2008). A presynaptic gain control mechanism fine-tunes olfactory behavior. Neuron 59, 311–321. <https://doi.org/10.1016/j.neuron.2008.07.003>.
87. Olsen, S.R., and Wilson, R.I. (2008). Lateral presynaptic inhibition mediates gain control in an olfactory circuit. Nature 452, 956–960. <https://doi.org/10.1038/nature06864>.
88. Task, D., Lin, C.C., Vulpe, A., Afify, A., Ballou, S., Brbic, M., Schlegel, P., Raji, J., Jeffreys, G., Li, H., et al. (2022). Chemoreceptor co-expression in *Drosophila melanogaster* olfactory neurons. eLife 11, e72599. <https://doi.org/10.7554/eLife.72599>.
89. Herre, M., Goldman, O.V., Lu, T.C., Caballero-Vidal, G., Qi, Y., Gilbert, Z.N., Gong, Z., Morita, T., Rahiel, S., Ghaninia, M., et al. (2022). Non-canonical odor coding in the mosquito. Cell 185, 3104–3123.e28. <https://doi.org/10.1016/j.cell.2022.07.024>.
90. Tumlinson, J.H., Klein, M.G., Doolittle, R.E., Ladd, T.L., and Proveaux, A.T. (1977). Identification of the female Japanese beetle sex pheromone: inhibition of male response by an enantiomer. Science 197, 789–792. <https://doi.org/10.1126/science.197.4305.789>.
91. Renou, M., and Guerrero, A. (2000). Insect pheromones in olfaction research and semiochemical-based pest control strategies. Annu. Rev. Entomol. 45, 605–630. <https://doi.org/10.1146/annurev.ento.45.1.605>.
92. Amoore, J.E., Palmieri, G., Wanke, E., and Blum, M.S. (1969). Ant alarm pheromone activity: correlation with molecular shape by scanning computer. Science 165, 1266–1269. <https://doi.org/10.1126/science.165.3899.1266>.
93. Roelofs, W.L., and Brown, R.L. (1982). Pheromones and evolutionary relationships of Tortricidae. Annu. Rev. Ecol. Syst. 13, 395–422. <https://doi.org/10.1146/annurev.es.13.110182.002143>.
94. Adams, S.A., and Tsutsui, N.D. (2020). The evolution of species recognition labels in insects. Philos. Trans. R. Soc. Lond. B 375, 20190476. <https://doi.org/10.1098/rstb.2019.0476>.
95. D'Ettorre, P., Errard, C., Ibarra, F., Francke, W., and Hefetz, A. (2000). Sneak in or repel your enemy: Dufour's gland repellent as a strategy for successful usurpation in the slave-maker *Polyergus rufescens*. Chemoecology 10, 135–142. <https://doi.org/10.1007/PL00001815>.
96. Lenoir, A., D'Ettorre, P., Errard, C., and Hefetz, A. (2001). Chemical ecology and social parasitism in ants. Annu. Rev. Entomol. 46, 573–599. <https://doi.org/10.1146/annurev.ento.46.1.573>.
97. Menzel, F., Blüthgen, N., Toliasch, T., Conrad, J., Beifuß, B., T., and Schmitt, T. (2013). Crematoenes – a novel substance class exhibited by ants functions as appeasement signal. Front. Zool. 10, 32. <https://doi.org/10.1186/1742-9994-10-32>.
98. Regnier, F.E., and Wilson, E.O. (1971). Chemical communication and "propaganda" in slave-making ants. Science 172, 267–269. <https://doi.org/10.1126/science.172.3980.267>.
99. Brandt, M., Heinze, J., Schmitt, T., and Foitzik, S. (2006). Convergent evolution of the Dufour's gland secretion as a propaganda substance in the slave-making ant genera *Protomognathus* and *Harpagoxenus*. Insect Soc. 53, 291–299. <https://doi.org/10.1007/s00040-006-0871-z>.
100. Dejean, A., Corbara, B., Roux, O., and Orivel, J. (2014). The antipredatory behaviours of Neotropical ants towards army ant raids (Hymenoptera: Formicidae). Myrmecol. News 19, 17–24.
101. Lloyd, H.A., Schmuff, N.R., and Hefetz, A. (1986). Chemistry of the anal glands of *Bothriomyrmex syrius* Forel. Olfactory mimetism and temporary social parasitism. Comp. Biochem. Physiol. B 83b, 71–73. [https://doi.org/10.1016/0305-0491\(86\)90333-0](https://doi.org/10.1016/0305-0491(86)90333-0).
102. Stoeffler, M., Maier, T.S., Toliasch, T., and Steidle, J.L. (2007). Foreign-language skills in rove-beetles? Evidence for chemical mimicry of ant alarm pheromones in myrmecophilous *Pella* beetles (Coleoptera: Staphylinidae). J. Chem. Ecol. 33, 1382–1392. <https://doi.org/10.1007/s10886-007-9315-0>.
103. Cattaneo, A.M., Gonzalez, F., Bengtsson, J.M., Corey, E.A., Jacquin-Joly, E., Montagné, N., Salvagnin, U., Walker, W.B., Witzgall, P., Anfora, G., et al. (2017). Candidate pheromone receptors of codling moth *Cydia*

- pomonella* respond to pheromones and kairomones. *Sci. Rep.* 7, 41105. <https://doi.org/10.1038/srep41105>.
104. Isogai, Y., Si, S., Pont-Lezica, L., Tan, T., Kapoor, V., Murthy, V.N., and Dulac, C. (2011). Molecular organization of vomeronasal chemoreception. *Nature* 478, 241–245. <https://doi.org/10.1038/nature10437>.
105. Allan, R.A., Elgar, M.A., and Capon, R.J. (1996). Exploitation of an ant chemical alarm signal by the zodariid spider *Habronestes bradleyi* Walckenaer. *Proc. R. Soc. Lond. B* 263, 69–73. <https://doi.org/10.1098/rspb.1996.0012>.
106. Uchida, N., Takahashi, Y.K., Tanifuji, M., and Mori, K. (2000). Odor maps in the mammalian olfactory bulb: domain organization and odorant structural features. *Nat. Neurosci.* 3, 1035–1043. <https://doi.org/10.1038/79857>.
107. Fishilevich, E., and Vosshall, L.B. (2005). Genetic and functional subdivision of the *Drosophila* antennal lobe. *Curr. Biol.* 15, 1548–1553. <https://doi.org/10.1016/j.cub.2005.07.066>.
108. Prieto-Godino, L.L., Rytz, R., Cruchet, S., Bargeton, B., Abuin, L., Silbering, A.F., Ruta, V., Dal Peraro, M., and Benton, R. (2017). Evolution of acid-sensing olfactory circuits in drosophilids. *Neuron* 93, 661–676.e6. <https://doi.org/10.1016/j.neuron.2016.12.024>.
109. Hölldobler, B. (1995). The chemistry of social regulation: multicomponent signals in ant societies. *Proc. Natl. Acad. Sci. USA* 92, 19–22. <https://doi.org/10.1073/pnas.92.1.19>.
110. Morgan, E.D. (2009). Trail pheromones of ants. *Physiol. Entomol.* 34, 1–17. <https://doi.org/10.1111/j.1365-3032.2008.00658.x>.
111. Bonavita-Cougourdan, A., Clément, J.L., and Lange, C. (1987). Nestmate recognition: the role of cuticular hydrocarbons in the ant *Camponotus vagus* Scop. *J. Entomol. Sci.* 22, 1–10. <https://doi.org/10.18474/0749-8004-22.1.1>.
112. Kleineidam, C.J., Obermayer, M., Halbich, W., and Rössler, W. (2005). A macroglomerulus in the antennal lobe of leaf-cutting ant workers and its possible functional significance. *Chem. Senses* 30, 383–392. <https://doi.org/10.1093/chemse/bji033>.
113. Butterwick, J.A., del Márml, J., Kim, K.H., Karlsson, M.A., Rogow, J.A., Walz, T., and Ruta, V. (2018). Cryo-EM structure of the insect olfactory receptor Orco. *Nature* 560, 447–452. <https://doi.org/10.1038/s41586-018-0420-8>.
114. Riabinina, O., Task, D., Marr, E., Lin, C.C., Alford, R., O'Brochta, D.A., and Potter, C.J. (2016). Organization of olfactory centres in the malaria mosquito *Anopheles gambiae*. *Nat. Commun.* 7, 13010. <https://doi.org/10.1038/ncomms13010>.
115. Schindelin, J., Arganda-Carreras, I., Frise, E., Kaynig, V., Longair, M., Pietzsch, T., Preibisch, S., Rueden, C., Saalfeld, S., Schmid, B., et al. (2012). Fiji: an open-source platform for biological-image analysis. *Nat. Methods* 9, 676–682. <https://doi.org/10.1038/nmeth.2019>.
116. Arzt, M., Deschamps, J., Schmied, C., Pietzsch, T., Schmidt, D., Tomančák, P., Haase, R., and Jug, F. (2022). LABKIT: labeling and segmentation toolkit for big image data. *Front. Comput. Sci.* 4, 777728. <https://doi.org/10.3389/fcomp.2022.777728>.
117. Bolger, A.M., Lohse, M., and Usadel, B. (2014). Trimmomatic: a flexible trimmer for Illumina sequence data. *Bioinformatics* 30, 2114–2120. <https://doi.org/10.1093/bioinformatics/btu170>.
118. Li, H. (2013). Aligning sequence reads, clone sequences and assembly contigs with BWA-MEM. . Preprint at arXiv. <https://doi.org/10.48550/arXiv.1303.3997>.
119. Li, H., Handsaker, B., Wysoker, A., Fennell, T., Ruan, J., Homer, N., Marth, G., Abecasis, G., and Durbin, R.; 1000 Genome Project Data Processing Subgroup (2009). The sequence alignment/map format and SAMtools. *Bioinformatics* 25, 2078–2079. <https://doi.org/10.1093/bioinformatics/btp352>.
120. R Core Team (2021). R: A Language and Environment for Statistical Computing (R Foundation for Statistical Computing). <http://www.R-project.org>.
121. Wickham, H. (2016). *ggplot2: Elegant Graphics for Data Analysis* (Springer-Verlag).
122. Robinson, J.T., Thorvaldsdóttir, H., Winckler, W., Guttman, M., Lander, E.S., Getz, G., and Mesirov, J.P. (2011). Integrative genomics viewer. *Nat. Biotechnol.* 29, 24–26. <https://doi.org/10.1038/nbt.1754>.
123. Bodenhofer, U., Bonatesta, E., Horejš-Kainrath, C., and Hochreiter, S. (2015). msa: an R package for multiple sequence alignment. *Bioinformatics* 31, 3997–3999. <https://doi.org/10.1093/bioinformatics/btv494>.
124. Larkin, M.A., Blackshields, G., Brown, N.P., Chenna, R., McGettigan, P.A., McWilliam, H., Valentin, F., Wallace, I.M., Wilim, A., Lopez, R., et al. (2007). Clustal W and Clustal X version 2.0. *Bioinformatics* 23, 2947–2948. <https://doi.org/10.1093/bioinformatics/btm404>.
125. Morgulis, A., Coulouris, G., Raytselis, Y., Madden, T.L., Agarwala, R., and Schäffer, A.A. (2008). Database indexing for production MegaBLAST searches. *Bioinformatics* 24, 1757–1764. <https://doi.org/10.1093/bioinformatics/btn322>.
126. Gel, B., and Serra, E. (2017). karyoploteR: an R/Bioconductor package to plot customizable genomes displaying arbitrary data. *Bioinformatics* 33, 3088–3090. <https://doi.org/10.1093/bioinformatics/btx346>.
127. Li, K. (2008). The image stabilizer plugin for ImageJ. http://www.cs.cmu.edu/~kangli/code/Image_Stabilizer.html.
128. Ravary, F., and Jaisson, P. (2004). Absence of individual sterility in thelytokous colonies of the ant *Cerapachys biroi* Forel (Formicidae, Ceraphyinae). *Insectes Soc.* 51, 67–73. <https://doi.org/10.1007/s00040-003-0724-y>.
129. Teseo, S., Châline, N., Jaisson, P., and Kronauer, D.J.C. (2014). Epistasis between adults and larvae underlies caste fate and fitness in a clonal ant. *Nat. Commun.* 5, 3363. <https://doi.org/10.1038/ncomms4363>.
130. Kronauer, D.J.C., Tsuji, K., Pierce, N.E., and Keller, L. (2013). Non-nest mate discrimination and clonal colony structure in the parthenogenetic ant *Cerapachys biroi*. *Behav. Ecol.* 24, 617–622. <https://doi.org/10.1093/beheco/ars227>.
131. Regnier, F.E., and Wilson, E.O. (1968). The alarm-defence system of the ant *Acanthomyops claviger*. *J. Insect Physiol.* 14, 955–970. [https://doi.org/10.1016/0022-1910\(68\)90006-1](https://doi.org/10.1016/0022-1910(68)90006-1).
132. Regnier, F.E., and Wilson, E.O. (1969). The alarm-defence system of the ant *Lasius alienus*. *J. Insect Physiol.* 15, 893–898. [https://doi.org/10.1016/0022-1910\(69\)90129-2](https://doi.org/10.1016/0022-1910(69)90129-2).
133. Ayre, G.L., and Blum, M.S. (1971). Attraction and alarm of ants (*Campnotus* spp.: Hymenoptera: Formicidae) by pheromones. *Physiol. Zool.* 44, 77–83. <https://doi.org/10.1086/physzool.44.2.3015558>.
134. Lenz, E.L., Krasnec, M.O., and Breed, M.D. (2013). Identification of undecane as an alarm pheromone of the ant *Formica argentea*. *J. Insect Behav.* 26, 101–108. <https://doi.org/10.1007/s10905-012-9337-5>.
135. Gibson, D.G., Young, L., Chuang, R.Y., Venter, J.C., Hutchison, C.A., and Smith, H.O. (2009). Enzymatic assembly of DNA molecules up to several hundred kilobases. *Nat. Methods* 6, 343–345. <https://doi.org/10.1038/nmeth.1318>.
136. Gibson, D.G., Glass, J.I., Lartigue, C., Noskov, V.N., Chuang, R.Y., Algire, M.A., Benders, G.A., Montague, M.G., Ma, L., Moodie, M.M., et al. (2010). Creation of a bacterial cell controlled by a chemically synthesized genome. *Science* 329, 52–56. <https://doi.org/10.1126/science.1190719>.

STAR★METHODS

KEY RESOURCES TABLE

REAGENT or RESOURCE	SOURCE	IDENTIFIER
Antibodies		
Chicken polyclonal anti-GFP	Abcam	Cat#ab13970; RRID: AB_300798
Rabbit polyclonal anti-RFP	Rockland	Cat#600-401-379; RRID: AB_2209751
Mouse monoclonal anti-SYNORF1	Developmental Systems Hybridoma Bank	DSHB: 3C11; RRID: AB_528479
Mouse monoclonal anti-Orco	Gift from Vanessa Ruta; Butterwick et al. ¹¹³	clone 20F7
Goat anti-Chicken Alexa 488	Invitrogen	Cat#A-11039; RRID: AB_2534096
Donkey anti-Mouse Alexa 647	Invitrogen	Cat#A32787; RRID: AB_2762830
Donkey anti-Rabbit Alexa 594	Invitrogen	Cat# A-21207; RRID: AB_141637
Chemicals, peptides, and recombinant proteins		
AlexaFluor 555 phalloidin	Invitrogen	Cat#A34055
DAPI	Invitrogen	Cat#D1306
Paraffin oil	Hampton Research	Cat#HR3-421
100% pentane	Sigma Aldrich	Cat#236705
96% 4-methyl-3-heptanone	Pfaltz and Bauer	Cat#M19160
≥ 99% 4-methyl-3-heptanol	Sigma-Aldrich	Cat#M48309
99% 6-methyl-5-hepten-2-one	Sigma-Aldrich	Cat#M48805-100ML
95% 4-methyl-3-hexanol	Enamine	Cat# 615-29-2
98% 3-hexanone	Aldrich Chemistry	Cat#103020-10G
98% ethylpyrazine	Sigma-Aldrich	Cat#250384-5G
99% propionic acid	Sigma-Aldrich	Cat#W292419-SAMPLE-K
100% ethanol	Decon Laboratories	Cat#2716
≥ 99.5% isopropanol	Fisher Chemical	Cat#A416SK-4
RNAClean SPRI XPBeads	Beckman Coulter	Cat#A63987
Critical commercial assays		
Endotoxin-free midiprep kit	Machery-Nagel	Cat#740420.10
HiScribe T7 Arca mRNA kit (with tailing)	New England Biolabs	Cat#E2060S
Experimental models: Organisms/strains		
<i>O. biroi</i> clonal line A wild type	Kronauer Lab	N/A
<i>O. biroi</i> clonal line B wild type	Kronauer Lab	N/A
<i>O. biroi</i> clonal line B [ie1-DsRed- ObirOrco-QF2-15xQUAS-GCaMP6s]; "GCaMP6s ant"	This paper	N/A
Deposited data		
<i>O. biroi</i> reference genome v5.4	McKenzie and Kronauer ¹⁰	GCA: 003672135.1
Whole-genome sequence of GCaMP6s ant	This paper	BioProject ID: PRJNA947257
Confocal microscopy data	This paper	Brain Image Library IDs: 7b20a5b168a92088; 626fd578e97289bc; c2031d8218de058b
Calcium imaging data	This paper	DANDI Archive ID: 000467
Oligonucleotides		
Primers for plasmid construction; see Table S4	This paper	N/A

(Continued on next page)

Continued

REAGENT or RESOURCE	SOURCE	IDENTIFIER
Recombinant DNA		
plasmid pGL3-IE1	Gift from Zach Adelman; Anderson et al. ⁶²	Addgene, ID 52894
plasmid pBAC-ECFP-15xQUAS_TATA-SV40	Gift from Christopher Potter; Riabinina et al. ¹¹⁴	Addgene, ID 104875
plasmid pBac-DsRed-ORCO_9kbProm-QF2	Gift from Christopher Potter; Riabinina et al. ¹¹⁴	Addgene, ID 104877
plasmid pGP-CMV-GCaMP6s	Gift from Douglas Kim & GENIE Project; Chen et al. ⁶⁰	Addgene, ID 40753
plasmid hyPB ^{apis}	Gift from Martin Beye; Otte et al. ⁶⁵	N/A
plasmid pBAC-ie1-DsRed-ObirOrco-QF2-15xQUAS-GCaMP6s	This paper	Addgene, ID 200400
Software and algorithms		
ImageJ (Fiji) version 2.0.0	Schindelin et al. ¹¹⁵	https://fiji.sc/
LABKIT plugin for ImageJ	Arzt et al. ¹¹⁶	https://github.com/juglab/labkit-ui
Trimmomatic 0.36	Bolger et al. ¹¹⁷	http://www.usadellab.org/cms/?page=trimmomatic
bwa mem	Li ¹¹⁸	https://github.com/lh3/bwa
Picard	Broad Institute	http://broadinstitute.github.io/picard/
samtools	Li et al. ¹¹⁹	https://github.com/samtools/samtools
R	R Core Team ¹²⁰	www.R-project.org
ggplot2	Wickham ¹²¹	https://ggplot2.tidyverse.org
Integrative Genomics Viewer	Robinson et al. ¹²²	https://software.broadinstitute.org/software/igv/
msa	Bodenhofer et al. ¹²³ ; Larkin et al. ¹²⁴	https://bioconductor.org/packages/release/bioc/html/msa.html
BLAST	Morgulis et al. ¹²⁵	https://blast.ncbi.nlm.nih.gov/Blast.cgi
karyoploteR	Gel and Serra ¹²⁶	http://bioconductor.org/packages/release/bioc/html/karyoploteR.html
Prism	GraphPad Prism	https://www.graphpad.com
Image Stabilizer plugin for ImageJ	Li ¹²⁷	http://www.cs.cmu.edu/~kangli/code/Image_Stabilizer.html
napari	napari contributors	Zenodo https://doi.org/10.5281/zenodo.3555620
Other		
Additional scripts	This study	https://github.com/Social-Evolution-and-Behavior/Hart_Kronauer2023

RESOURCE AVAILABILITY

Lead contact

Further information and requests for resources and reagents should be directed to and will be fulfilled by the lead contact, Daniel J.C. Kronauer (dkronauer@rockefeller.edu).

Materials availability

The plasmid used for generating the GCaMP6s ants has been deposited to Addgene (accession # 200400).

Data and code availability

- DNA sequence data have been deposited to NCBI BioProject. Confocal microscopy data have been deposited to the Brain Image Library. Calcium imaging data have been deposited to the DANDI Archive. Accession numbers are listed in the [key resources table](#).

- All original code has been deposited to GitHub and the repository is listed in the [key resources table](#).
- Any additional information required to reanalyze the data reported in this paper is available from the [lead contact](#) upon request.

EXPERIMENTAL MODEL AND STUDY PARTICIPANT DETAILS

Ant husbandry and maintenance

Ants were kept at 25°C in nests constructed by lining 5cm diameter Petri dishes with plaster of Paris. Nests were kept humidified and supplied with frozen fire ant pupae as food ~3 times per week during the brood care phase. Petri dishes held 20-80 workers each. GCaMP6s ants were propagated by cross-fostering GCaMP6s eggs into colonies with clonal line A adults,¹² which were then separated into isogenic GCaMP6s colonies after eclosion. Isogenic colonies can easily be assembled in this species because *O. biroi* reproduces clonally.^{45,128} We separated transgenic animals at the G1 stage and returned all offspring of a particular G1 individual to the same nest as their parent. For live imaging experiments, stock colonies for experiments were assembled by moving cohorts of cross-fostered GCaMP6s ants that eclosed within 2 weeks of one another into fresh Petri dish nests. Adult female ants were selected from stock colonies for GCaMP imaging experiments. The age of experimental ants was 55-60- and 90-104 days post eclosion for the general odorant and alarm pheromone imaging experiments, respectively. Individuals with eyespots (indicative of intercastes)^{129,130} were excluded from our imaging study.

METHOD DETAILS

Behavior

Alarm pheromones

We purchased 96% 4-methyl-3-heptanone from Pfaltz and Bauer (Item # M19160), and ≥99% 4-methyl-3-heptanol and 99% 6-methyl-5-hepten-2-one from Sigma-Aldrich (Item # M48309 and M48805-100ML, respectively). 95% 4-methyl-3-hexanol was purchased from Enamine (CAS # 615-29-2), and paraffin oil from Hampton Research (cat. # HR3-421). We also initially tested the compound undecane, which functions as an alarm pheromone in several other ant species and is found in clonal raider ant extracts.^{22,131-134} However, undecane has a lower volatility / vapor pressure than the other alarm pheromones (Table S3), and only elicited non-specific walking behavior and no robust calcium responses in our experimental paradigms. We therefore did not investigate undecane further.

General odorants

98% 3-hexanone was purchased from Aldrich Chemistry (Item # 103020-10G). 98% ethylpyrazine and 99% propionic acid were purchased from Sigma-Aldrich (Item # 250384-5G and W292419-SAMPLE-K, respectively). 100% ethanol was purchased from Decon Laboratories (Item # 2716), and ≥99.5% isopropanol from Fisher Chemical (Item # A416SK-4). We initially also tested six additional general odorants with lower volatility / vapor pressure (Table S3). However, these odorants did not elicit robust calcium responses in our experimental paradigm and were therefore not studied further.

Colony alarm bioassay

Alarm behavior assays were performed as described previously.²² For experiments with 4-methyl-3-hexanol and 6-methyl-5-hepten-2-one, 30 mixed-age ants from clonal line B were introduced without brood into each arena. Trials were also performed with undecane, which only induced non-specific walking behavior. For behavioral experiments with GCaMP6s ants, due to limited numbers, 15-20 ants were introduced into each arena. Prior to behavioral experiments, ants were allowed to settle for at least 5 days, until they had laid eggs and spent most of their time within a tightly packed nest pile.

Each compound (pure compounds for 4-methyl-3-heptanone, 4-methyl-3-heptanol, 4-methyl-3-hexanol, 6-methyl-5-hepten-2-one, or a 9:1 4-methyl-3-heptanone:4-methyl-3-heptanol blend) was freshly diluted 1:20 with 100% pentane each day of experiments. After recording baseline activity for 4 minutes and 30 seconds, 50 µL of each compound was added to a ~1 cm² piece of filter paper and allowed to evaporate for 30 seconds before folding and placing into the stimulus chamber. Behavioral responses were recorded for another 5 minutes.

Data were analyzed as described previously, scoring three metrics of interest by hand: (1) the number of ants outside the nest pile, (2) the number of ants outside the nest chamber, and (3) the number of ants touching the mesh wall. We limited statistical analyses to the time window starting 1 minute prior to adding the stimulus and 2 minutes after. To evaluate the effect of the stimulus over time, we performed a two-way repeated measures ANOVA, and to determine the effect of the stimulus at each timepoint we used Dunnett's multiple comparisons test.

Categorical analysis of the major behavioral response to each odorant (4-methyl-3-hexanol, 6-methyl-5-hepten-2-one, and the vehicle control, plus reanalysis of responses to 4-methyl-3-heptanone, 4-methyl-3-heptanol, and the blend from experiments in a previous study²²) was performed by visually classifying each video as one of the following in a blinded manner: "Immediate panic alarm": The nest pile was disassembled within one minute following stimulus exposure. "Ants leave nest": The nest pile persisted for at least one minute following stimulus exposure, but over half the ants left the nest pile within the first minute. "No immediate response": The nest pile persisted for at least one minute following stimulus exposure, and fewer than half the ants left the nest pile within the first minute. We also identified the time when the initial nest pile disappeared after addition of the stimulus. Because

we could not discern the removal of single eggs from the nest pile from the video, for the purposes of this analysis the nest pile was considered to persist as long as the same area continued to contain at least one egg and two adult ants. We calculated the percentage of time during which the initial nest pile persisted for the first two minutes after addition of the stimulus. We evaluated the effect of the compounds on the nest pile dissipating using a one-way ANOVA and Šídák's multiple comparisons test to compare each additional alarm pheromone to each of the two known *O. biroi* alarm pheromones (4-methyl-3-heptanone, 4-methyl-3-heptanol, and a 9:1 blend of the two compounds). Statistical analyses on behavioral data were performed using GraphPad Prism Version 9.4.0 for Windows, GraphPad Software, San Diego, California, USA (<https://www.graphpad.com>).

Generation of transgenic ants

Cloning and plasmid assembly

We assembled plasmid pBAC-ie1-DsRed-ObirOrco-QF2-15xQUAS-GCaMP6s using multiple rounds of PCR for generating fragments, restriction digestion with gel purification for backbones, and Gibson assembly cloning.^{135,136} Following each Gibson assembly step, correct assembly was verified using restriction digests and by sequencing PCR amplicons spanning across each of the fragment boundaries. Primer sequences for plasmid construction are listed together in Table S4. A plasmid schematic was made using MacVector software, MacVector Inc, Apex, North Carolina, USA (<https://macvector.com>).

- [1] ObirOrco: A 2.4kb promoter/enhancer fragment, including intergenic sequence and the entire 5' UTR, amplified from clonal raider ant genomic DNA, clonal line B (NCBI LOC105284785) (primers: forward, 5'- tagtgtgggttgttcgcacaTATGTCACGTA
ATCAGCTTTGACG -3', lowercase shows Gibson homology region; reverse 5'- gcgcgtgggtggcatgtgcaTCATATGTCTGCGA
GCAAATGGAACG -3').
- [2] piggyBac backbone from pBAC-ECFP-15xQUAS_TATA-SV40 (Addgene, ID #104875),¹¹⁴ from double restriction digest with SpeI (New England Biolabs [NEB] #R3133S) and EcoRV (NEB #R0195S).
- [3] ie1-A: An enhancer/promoter from pGL3-IE1 (Addgene ID #52894)⁶² (primers: forward 5'- ttatcgaattccctgcagccccggggatc
caACTAGTTGTCGCCGAGCTTACGCGC -3', reverse 5'- ctggaggaggccatCCGCAGCGAACAGGTCACTGGTTGTT
CACGATCTTG -3').
- [4] DsRed from pBac-DsRed-ORCO_9kbProm-QF2 (Addgene ID #104877)¹¹⁴ (primers: forward 5'- acctgttgcggcgAT
GGCCTCTCCGAGAA -3', reverse 5'- ttattatataatttctgttatagatGGCGCGCCGAACACATATGCGAACAAACAAACCAA
CTAGAATGCAGTG -3').
- [5] QF2 from pBac-DsRed-ORCO_9kbProm-QF2 (primers: forward 5'- aaccaagtgacactgttgcggcgACATATGCAACATGC
CACCCAA -3', reverse 5'- acccagtgacacgtgacccCGAGCGCTGGATCTAAACGAGTTTAAGC -3').
- [6] 15xQUAS from pBAC-ECFP-15xQUAS_TATA-SV40 (primers: forward 5'- cggcacgtgtcact -3', reverse 5'- tgagaaccatcgaa
caagcGTTAACAGATCTGTTAACGAATTGATC -3').
- [7] GCaMP6s from pGP-CMV-GCaMP6s (Addgene ID # 40753)⁶⁰ (primers: forward 5'- gggccggccgttcgAGCGCTTTCGAT
GGGTTCTCATCATCATC -3', reverse 5'- atatatttctgttatagatggCGCGCCGTAGCCCTAACGATACATTGATGAGTTTG -3')
- [8] pBAC-ie1-DsRed from Gibson assembly of piggyBac backbone, ie1-A, and DsRed fragments, transformed into NEB 10-beta competent cells (item # C3019H).
- [9] ie1-B from pBAC-ie1-DsRed, (primers: forward 5'- ctgcattctagttgggttgttcgaCATATGTGTCGCCGAGCTTACGCG
-3', reverse 5'- catcgaacaagcgctgaacaggcccccGAACAGGTCACTGGTTTCAC -3')
- [10] pBAC-ie1-DsRed-ie1-GCaMP6s from Gibson assembly of pBAC-ie1-DsRed (linearized using double restriction digest with NdeI [NEB #R0111S] and Ascl [NEB #R0558S]), ie1-B, and GCaMP6s.
- [11] pBAC-ie1-DsRed-ie1-QF2-15xQUAS-GCaMP6s from Gibson assembly of pBAC-ie1-DsRed-ie1-GCaMP6s (linearized using double restriction digest with FseI [NEB #R0588S] and Afel [NEB # R0652S]), QF2, and 15xQUAS.
- [12] pBAC-ie1-DsRed-ObirOrco-QF2-15xQUAS-GCaMP6s from Gibson assembly of pBAC-ie1-DsRed-ie1-GCaMP6s (linearized and second ie1 copy removed using restriction digest with NdeI) and ObirOrco.

Preparation of injection mixes

Plasmid DNA for injection was purified using a Machery-Nagel endotoxin-free midiprep kit (item #740420.10). The final pellet was washed under RNAse-free conditions and dissolved in nuclease-free water. To remove precipitated DNA from injection mixes, the dissolved plasmid mix was spun in a microcentrifuge at top speed for 5 minutes, and the top 90% of the supernatant was recovered. This step was repeated at least 5 times to produce injectable mix with negligible precipitate, which was stored at -20°C until injection.

We generated mRNA from the hyperactive piggyBac variant hyPBase^{apis}.⁶⁵ A DNA template was generated by PCR amplification of the transposase coding sequence, with addition of a T7 promoter on the forward PCR primer, then purified using Beckman Coulter RNAClean SPRI XPBeads (item #A63987). In vitro transcription was performed with the NEB HiScribe T7 Arca mRNA kit (with tailing) (item #E2060S) to produce poly(A) tailed mRNA encoding hyPBase^{apis}. The mRNA was purified using RNAClean beads (using 1.5x volume of beads compared to the reaction mix) and stored in nuclease-free water at -80°C. Template and RNA were handled under RNase-free conditions, and a sample of mRNA was examined on an Agilent Bioanalyzer to verify RNA length and confirm absence of degradation. All DNA and RNA concentrations were measured using a Thermo Fisher Nanodrop.

Egg collection, microinjection, and larval rearing

Eggs were collected as described previously,¹² with a modified schedule for treatments with eggs <3 hours old. We tested the effect of injecting even younger eggs than our previous protocol which used eggs <5 hours old¹² so that hyPBBase^{apis} mRNA could be translated into active transposase while embryos still had very few nuclei, potentially reducing mosaicism. For these treatments, old eggs were removed from nests from 9am-10am, and eggs for injection were collected from 11am-11:30am, 1pm-1:30pm, 3pm-3:30pm, and 5pm-5:30pm. Injections were performed from 11:30am-12:30pm, 1:30pm-2:30pm, 3:30pm-4:30pm, and 5:30pm-6:30pm. This schedule meant that the vast majority of eggs were less than 3 hours old when injected.

Microinjections were performed as described previously,¹² with the following changes: On each injection day, final injection mixes were produced by thawing and combining stored aliquots of plasmid DNA and hyPBBase^{apis} mRNA under RNase-free conditions in nuclease-free water, into a final concentration of 27.8pmol/μL plasmid and the desired concentration of hyPBBase^{apis}. The injected plasmid had a length of 12,025bp. The final mix was spun at top speed in a microcentrifuge for 5 minutes, and the top 90% of supernatant was used for injection. The initial mix was split into 4 aliquots and kept on ice for the day. A different aliquot was used for each round of injections. On occasions where the needle clogged, the mix was spun at top speed in a microcentrifuge before loading a new needle. The injection pressure was initially set to 3600kpa but was adjusted throughout the course of injections to maintain a consistent flow of liquid into the embryos. We varied the age of eggs and the concentration of transposase mRNA in the injection mix. Higher rates of fluorescent G0s were obtained when eggs were <3 hours old rather than <5 hours old at the time of injection. Mixes with >110ng/μL mRNA concentrations produced low hatch rates and no fluorescent G0s (Table 1).

Larvae were reared as described previously.¹² Briefly, G0 larvae were hatched and placed in small colonies housed in 5cm diameter Petri dishes with a moist plaster of Paris floor to be reared by adult ants from clonal line A, which we refer to as “chaperones” when we use them to rear offspring transferred from other colonies.¹² Colonies were examined under an epifluorescence microscope to confirm that some larvae expressed DsRed, indicating uptake of the plasmid.

Rearing initial transgenic populations

G0 individuals were reared to adulthood. For cohorts of sufficient size (~20 individuals), chaperones were removed. When the number of G0s was too small to form a robust colony, they were supplemented with wild type clonal line A ants to obtain a population of ~20 individuals. One hind leg was removed from each wild type ant to reduce their egg-laying rate compared to the G0 ants in the nest. Then, the colonies were allowed to produce G1 eggs, which were usually collected twice a week. Collected eggs were transferred to a small colony of ~20 chaperones. G1 individuals were reared to adulthood in these nests and were examined for fluorescence. Different G1 individuals potentially resulted from independent transgene insertion events. To ensure that future transgenic populations were genetically homogeneous, each fluorescent G1 adult was separated soon after eclosion, and transferred to a new transgenic line-founding colony with ~19 clonal line A ants. Eggs were collected about twice a week from these nests and given to chaperones. Fluorescent adults produced from these colonies were then returned to the transgenic line-founding colony of origin. Through several cycles of this process, genetically homogenous transgenic populations were raised and non-fluorescent individuals were removed, yielding pure colonies.

Phenotyping transgenic ants

Fluorescence microscopy

Confocal microscopy of antibody-stained tissue was conducted using Zen image acquisition software on a Zeiss LSM 880 and a Zeiss LSM 900 equipped with 405nm, 488nm, 561nm and 633nm laser lines. Images were obtained using either a Zeiss LD LCI Plan-Apochromat 40X / 1.2NA or a Zeiss LD LCI Plan-Apochromat 25X / 0.8NA multi-immersion objective lens depending on the tissue sample and Zeiss Immersol G immersion medium (Zeiss # 462959-9901-000). Z-projection images were produced from stacks taken at 1 μm steps using ImageJ/FIJI.¹¹⁵ Two-photon fluorescence microscopy was performed using a Bruker Investigator with a Coherent Axon laser tuned to 920nm, equipped with dual GaAsP detectors, resonant scanning galvanometer, Z-piezo module for high-speed Z-positioning, PrairieView software, and an Olympus 40X 0.9NA water-immersion objective. Images of transgenic pupae (Figure 1B) were produced on an Olympus SZX16 epifluorescent microscope equipped with an X-Cite XYLIS light source, Olympus EP50 camera, and the appropriate filter cubes.

Immunohistochemistry

Antibody staining of ant brains was performed as reported previously.⁹ Briefly, the brains of female ants of a single-age cohort were dissected in cold phosphate-buffered saline (PBS) and fixed in 4% paraformaldehyde for 2 hours at room temperature. For antenna staining, a small section of cuticle was mechanically separated prior to fixation to enhance access. Blocking was performed for at least 2 hours using fresh PBS containing 0.1% or 0.5% Triton X-100 and 5% donkey serum albumin. Samples were incubated with the appropriate dilution of primary antibody in fresh blocking solution on an orbital shaker table at room temperature. Following primary incubation, samples were washed and incubated with fluorescently tagged secondary antibody diluted in fresh blocking solution. The following antibodies were used: chicken anti-GFP (Abcam #ab13970), rabbit anti-RFP (Rockland #600-401-379), mouse anti-SYNORF1 (DSHB #3C11), mouse anti-Orco (gift from V. Ruta), goat anti-chicken Alexa 488 (Invitrogen #A-11039), donkey anti-mouse Alexa 647 (Invitrogen #A32787), and donkey anti-rabbit Alexa 594 (Invitrogen # A-21207). For some experiments, DAPI (Invitrogen #D1306) and fluorescently tagged phalloidin (Invitrogen #A34055) were included during the secondary antibody incubation step. Stained tissue was mounted in SlowFade mounting medium on silane-coated microscopy slides (VWR #63411-01) and stored at 4°C. For the high quality anatomical AL reconstruction, a confocal stack of the right AL from a GCaMP6s-positive brain stained with

anti-SYNORF1 was manually segmented using the LABKIT plugin for ImageJ, at $1\mu\text{m}$ z-axis resolution.^{115,116} To quantify overlap between GCaMP and Orco expression, a second AL reconstruction was performed using the left AL of a GCaMP6s-positive brain stained with anti-Orco and phalloidin. All glomeruli were reconstructed and then checked for GCaMP6s/anti-Orco/phalloidin signal. The T7 glomerulus cluster was identified by its anatomical position and lack of Orco antibody staining, as described previously.¹¹ Renders of the reconstructed ALs (Figures S2A and S2B) were generated using napari (Zenodo <https://doi.org/10.5281/zenodo.3555620>). While examining brains one month after unilateral antennal ablation, we noticed that the AL associated with the ablated antenna appeared smaller than the AL associated with the intact antenna. We therefore reconstructed AL volumes from several brains ($n=3$) and found a non-significant trend toward smaller volumes on the ablated side (means of $165,360\mu\text{m}^3$ and $209,412\mu\text{m}^3$ for ablated vs. non-ablated ALs, respectively; $p=0.073$, paired values T-test). We did not investigate this phenomenon further.

Genome sequencing and genomic analyses

A single GCaMP6s ant was disrupted with a Qiagen TissueLyser II, and genomic DNA was extracted using a Qiagen QIAamp DNA Micro Kit. Libraries were prepared using Nextera Flex, and paired end, 150 base pair reads were sequenced on an Illumina NovaSeq S1 Flow Cell. Raw reads were trimmed using Trimmomatic 0.36¹¹⁷ and aligned using bwa mem¹¹⁸ to both the *O. biroi* reference genome (Obir_v5.4, GenBank assembly accession: GCA_003672135.1)¹⁰ and a linearized plasmid reference genome created by “cutting open” the plasmid sequence at an arbitrary location on the backbone, and pasting 150 bp from the end at the front of the sequence and 150 bp from the front at the end of the sequence to accommodate any reads that might align to the vicinity of the “cut”. Reads were sorted and deduplicated using Picard (<http://broadinstitute.github.io/picard/>), and read depth was recorded at all sites using “samtools depth -aa”¹¹⁹ (obtaining approximately 44x coverage). To infer the read depth of well-assembled genomic regions, we obtained all heterozygous SNPs with read depth less than 2x the genome-wide median, which excluded the fewer than 0.5% of such SNPs which likely resulted from errors in genome assembly. We then randomly selected an equal number of heterozygous SNPs as the number of base pairs in the transgene insert, and calculated read depth at those sites, and separately along both the portion of the transgene insert sequence that aligned to ObirOrco and the rest of the transgene insert. Data in Figure S3A were plotted using the R package ggplot2.^{120,121}

Junction reads that aligned to both the transgene insert and the *O. biroi* reference genome were identified using the Integrative Genomics Viewer,¹²² and alignments were queried by each junction read name using “samtools view”.¹¹⁹ We performed multiple sequence alignment on these junction reads from each end of the insert using CLUSTAL 2.1 in the R package msa^{120,123,124} and generated consensus sequences. To obtain the sequence of the insertion site in the reference genome, the portion of the sequence that was identical to the end of the transgene insert sequence was removed from the junction read consensus sequences. BLAST¹²⁵ searches of the partial consensus sequence identified a position consistent with the position these junction reads had aligned to in the *O. biroi* reference genome. Figure S3B was generated using the R package karyoploteR.¹²⁶ The insertion locus was examined in the NCBI genome data viewer (Obir_v5.4, GenBank assembly accession: GCA_003672135.1)¹⁰ to check for the presence of predicted gene models.

In vivo calcium imaging

Specimen preparation

Ants for live imaging were anesthetized on ice for ~3 minutes and then fastened to a custom two-photon imaging mount using blue-light curable glue. The antennae were restrained with a thin strip of Parafilm to decrease motion artifacts. A sheet of Parafilm with a hole for the ant's head was applied on top of the preparation, and a watertight seal was created around the border of the head using additional glue. The preparation was then bathed with fresh ant saline (127 mM NaCl, 7 mM KCl, 1.5 mM CaCl₂, 0.8 mM Na₂HPO₄, 0.4 mM KH₂PO₄, 4.8 mM TES, 3.2 mM Trehalose, pH 7.0)²⁶ and suffused for the duration of the imaging session with additional ant saline to prevent desiccation, before excising a small imaging window in the cuticle using a sterile hypodermic needle and sharp forceps. The window was positioned above the brain, and connective and glandular tissue were removed to reveal the antennal lobes. We always imaged the right antennal lobe. Care was taken to keep the antennae and antennal nerves intact. In some cases, a muscle between the ALs and near the esophagus was severed, which reduced the amount of brain motion. This was advantageous for imaging, but not always feasible due to the small distance between the ALs and slight differences in the accessibility of the muscle from ant to ant.

Two-photon recording

Antennal lobe volumes were recorded at 2X optical zoom and a resolution of 512x512x33 voxels (XYZ) with $5\mu\text{m}$ Z steps, resulting in a volume with dimensions of $148\mu\text{m} \times 148\mu\text{m} \times 165\mu\text{m}$, large enough to capture calcium transients from the entire AL which has approximate dimensions of $65\mu\text{m} \times 125\mu\text{m} \times 150\mu\text{m}$. As glomeruli are typically spheroid with a diameter of $10\text{-}20\mu\text{m}$, each glomerulus was captured in many voxels in all three dimensions. Recordings were obtained at 27.5 frames per second, resulting in 0.83 volumes per second. At the beginning of each imaging experiment, we located the dorsal surface of the AL and set that as the top of the imaging volume. We could clearly detect the boundary at the ventral surface of the AL where GCaMP6s signal disappeared, indicating that we imaged all GCaMP6s-positive glomeruli. Laser power and gain were adjusted for each ant so that all glomeruli were visible, but signal was unsaturated. Because we imaged at different depths, we compensated for loss of signal through tissue by increasing the laser power at greater depth using an exponential function. We regularly re-calibrated the position of the imaging volume, laser power, and gain in case there were any changes in baseline fluorescence or brain position during the experiment. The bilateral

calcium imaging experiment was conducted at 1X optical zoom, resulting in an imaging volume with dimensions of 296 μ m x 296 μ m x 165 μ m.

Stimulus presentation

Odors were presented using a custom-built olfactometer on 600mL/min of filtered, medical-grade air regulated with a pair of digital mass flow controllers (AliCat# MC-1SLPM-D-IPC/5M). A constant 'carrier' air stream (200mL/min) was presented to the ant for the duration of the imaging session to reduce mechanical stimulation of the antennae resulting from air turbulence, while a 'stimulus' portion of the air stream (400mL/min) was diverted and perfumed before rejoining the carrier stream at a manifold immediately upstream of the imaging preparation. By default, stimulus air bypassed control and odor vials and entered the manifold directly. During stimulus presentation, the air was perfumed by triggering high-speed three-way valves (Grainger# 6JJ52) controlled by an Arduino Uno and custom MatLab scripts, which directed the air to control or odor vials. Imaging and stimulus trials were synchronized in time using Bruker PrairieView software (i.e., the same TTL signal initiated both imaging and odor stimulation). Odors were dissolved in paraffin oil vehicle to a total volume of 300 μ L (concentrations represent v/v in the vial), were stored in 4mL amber glass vials with PTFE/silicone septa and connected to valves and the odor manifold via sterile hypodermic needles and nylon Luer tapers. Odor vials were prepared at the beginning of each day of imaging experiments. The air stream was directed onto the ant's antennae using flexible PVC/vinyl tubing with an internal diameter of 1.588mm (United States Plastic Corp. Item #: 54411) from a distance of approximately 1mm.

All odor presentations had a 3s lead time and lasted for 5s. Before odor presentation, we presented the ant with the paraffin oil vehicle as a negative control and confirmed the absence of fluorescence changes before continuing the experiment. For the general odorant imaging experiment, each ant was then presented with a randomized sequence of 7-9 general odorants (48.0% concentration) which was repeated for three trials. Each of the odorants in the panel was tested in 2-6 ants. Odorants: 3-hexanone, butyric acid, dodecyl acetate, ethanol, ethylpyrazine, geranyl acetate, isopropanol, linalool, propionic acid, terpineol, and (+)-valencene. Only responses to the 5 odorants that generated robust calcium responses that were consistent across ants are shown in Figure 3. We sometimes observed calcium activity from the other odorants, but responses were weak and not reproducible across trials in different ants. For the alarm pheromone imaging experiment, we first presented each ant with the paraffin oil vehicle and then with a positive control isopropanol stimulus. We only continued experiments with animals that showed calcium responses to the positive control but not the negative control. Each ant was presented with the four alarm pheromones in a random sequence which was first repeated for three trials at the lower concentration, followed by three additional trials at the higher concentration (for a total of 24 pheromone presentations per animal). Additional trials were performed with undecane, but these trials were not analyzed further due to absence of robust calcium responses. To reduce the impact of habituation to stimulus, each ant was presented with odors at two concentrations out of four concentrations tested (n=13 ants total, 3 ants presented with 0.75% and 12.0% odor concentrations; 2 ants with 3.0% and 12.0%; 3 ants with 12.0% and 48.0%; and 5 ants with 3.0% and 48.0%). In rare cases, we observed large motion artifacts during a recording, in which case the trial was repeated. For the bilateral calcium imaging experiment, ants were presented only with the paraffin oil vehicle and 4-methyl-3-hexanol at 48.0%. Vials and caps were reused after cleaning as follows: removal of remaining liquid, 2x wash with 100% ethanol alternating with 2x rinse in distilled water, 2x wash with 3% Alconox alternating with 2x rinse in distilled water, 2x rinse in distilled water, air dry.

Image processing and analysis

Image processing was done in Fiji/ImageJ.¹¹⁵ To initially characterize response to odorants, we loaded recordings, used the "Deinterleave" function to separate them into 33 slices corresponding to videos of each recording depth, ran the Image Stabilizer plugin,¹²⁷ applied the "Gaussian Blur" filter with 1-sigma, calculated F_0 from the mean of frames 1-5 (before any calcium changes were detected) and calculated $\Delta F/F_0$ by subtracting and then dividing the image stack from F_0 . The peak fold change was calculated using the "Z Project" function set to average the $\Delta F/F_0$ from frames 9-14, when the calcium responses typically peaked. After applying a pseudocolor LUT, we examined the peak fold change at all 33 depth positions to get a sense of the organization of glomerular responses across the ALs. We determined that all responses were positive and responding glomeruli were generally well-separated in the x/y axes. We performed additional analyses using max z-projections. Z-projections were generated by running image stabilization on each imaging plane,¹²⁷ computing $\Delta F/F_0$, running the "Minimum" filter with 2-pixel radius to reduce noise, applying the "Z Project" function through all slices with maximum setting, and changing all values >4 to 4 or <-1 to -1 using the "changeValues" function, to equalize the LUT range. To analyze glomerular response patterns across the whole AL, we examined all max z-projection images at the highest odor concentration for each ant and drew regions of interest (ROIs) around every glomerular region that responded to any odor in at least two trials (a small number of trials were excluded due to large motion artifacts that were only apparent after generating max projections). We then quantified the peak fold change across all trials for a particular odor and concentration and designated an ROI as responding if the value was ≥ 0.2 . In cases where two odors activated ROIs that overlapped in the max z-projection, we examined the z-stacks to determine if the responses occurred at the same z-depth and excluded overlaps if the responses occurred at different depths. For visualizing the imaging volume (Figure 3E, top), we used the first frame of a recording, and generated max z-projections using the z-project function. For the x-projection, we used the "Re-slice" function starting from the left to re-order the pixels, and then used the max z-project function. To visualize calcium responses throughout the imaging volume (Figure 3E, bottom), the max z-projections of calcium responses were generated as before, but because imaging noise was more apparent in the x-projections due to higher resolution in that axis compared to the z-axis, the minimum filter was set to a 3-pixel radius.

For analyses of single glomeruli, we visually identified the z-plane containing the center of the glomerulus of interest for each trial, generated a max z-projection across 3 adjacent imaging planes (to reduce the impact of brain motion in the z-axis), and then calculated $\Delta F/F_0$. Peak fold change was quantified by averaging the $\Delta F/F_0$ over frames 9–14, the time range during which most odor-evoked calcium responses peaked.

Spatial relationships between PG_b, PG_a, and 6G were quantified by examining a video z-plane in which all three glomeruli were visible, placing a marker at the center of each glomerulus, and calculating the vector connecting the centers, with PG_b at (0,0). In two individuals, the spatial relationship between PG_b and PG_a was not quantified because PG_a could not be identified.

Statistical analyses of odor responses

We analyzed the responses of the three glomeruli PG_b, PG_a, and 6G to different odors and concentrations. For every glomerulus/odor combination, peak fold change values from all trials were loaded into R, and a linear regression model was fit for the peak calcium response as a function of odor concentration, with a random effect for individual, using the `glm` function.¹²⁰ Model predictions were generated and plotted with `ggplot2`¹²¹ with 95% confidence intervals.

To examine temporal dynamics in the three focal glomeruli, normalized calcium response traces from each glomerulus were loaded into R.¹²⁰ The first five recorded frames were used as the baseline, and calcium response onset was defined as the latency between the start of the stimulus presentation and the time point where $\Delta F/F_0$ exceeded the mean of the baseline + 3SD of the baseline. The time to response maximum was defined as the latency between the start of the stimulus presentation and the timepoint with the maximum value of $\Delta F/F_0$. Traces where $\Delta F/F_0$ never exceeded the mean of the baseline + 3SD of the baseline were excluded. Only glomerulus/pheromone combinations with typically robust responses were included (4-methyl-3-heptanone in PG_b; 4-methyl-3-heptanol and 4-methyl-3-hexanol in PG_b and PG_a; 6-methyl-5-hepten-2-one in 6G). Data were plotted with `ggplot2`.¹²¹ To test for effects of pheromone and glomerulus identity on calcium response temporal dynamics, we performed statistical analyses on the subset of data for which the same pheromone caused responses in more than one focal glomerulus, i.e., responses in PG_b and PG_a from trials with 4-methyl-3-heptanol and 4-methyl-3-hexanol. For each temporal parameter, we built a linear mixed effects model using the `lme` function in R,¹²⁰ modeling the effects of pheromone, glomerulus, and an interaction of pheromone/glomerulus, with a random effect for trial ID nested within ant ID.

QUANTIFICATION AND STATISTICAL ANALYSIS

Analyses of behavioral data were performed using PRISM (GraphPad) ([Figures 1C–1F](#) and [S2C–S2F](#); [Table S2](#)). Analyses of genomic data were performed using software as described and cited above ([Figure S3](#)). Analyses of calcium imaging data were performed using R and the packages as described and cited above ([Figures 3D, 5C, 5D, S4C, S5, S6, and S7](#)). Data are presented as mean \pm SEM, mean \pm SD, or in another format as indicated in the relevant figure legends.

Supplemental figures

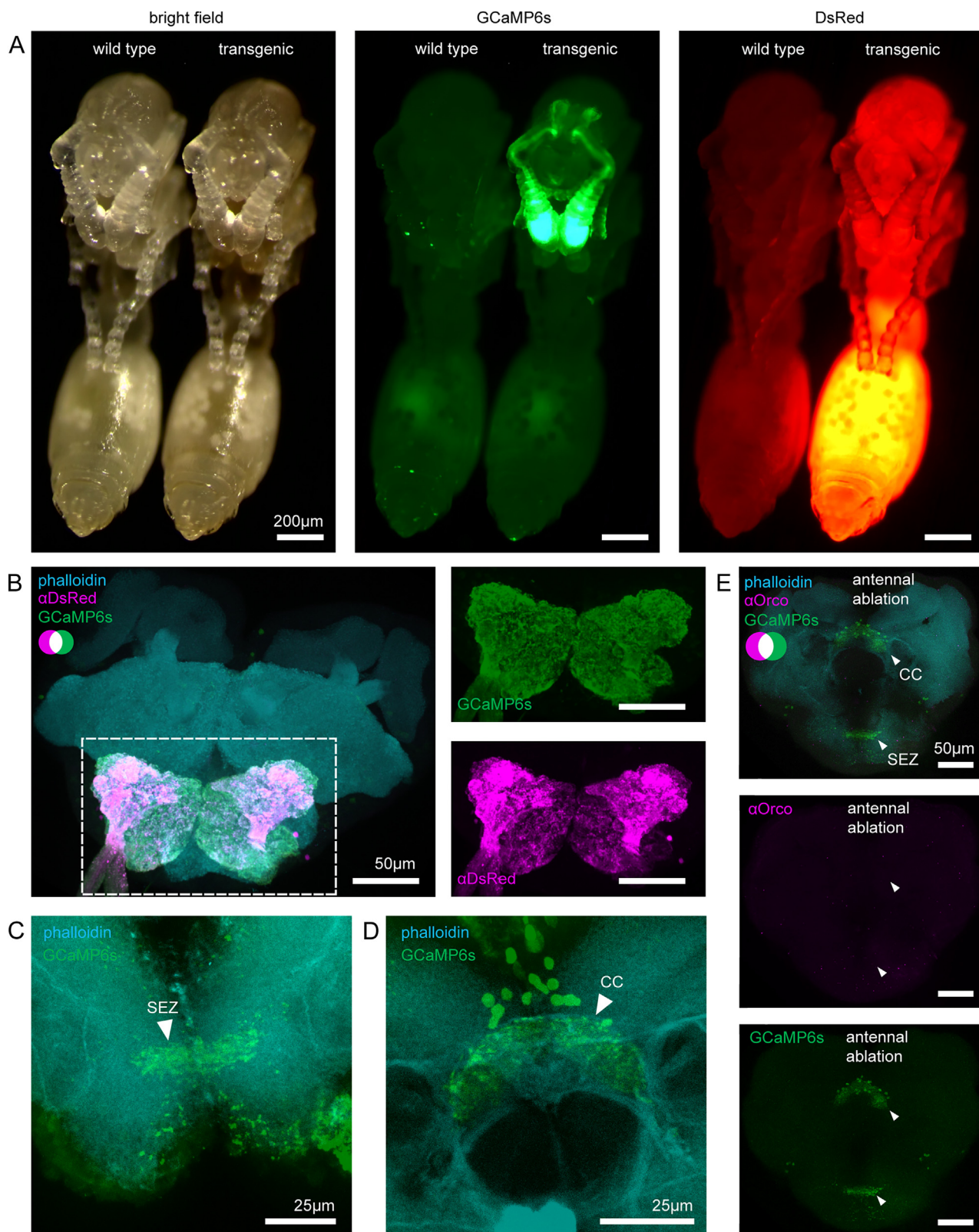


Figure S1. Additional characterization of GCaMP6s ants, related to Figure 2

- (A) The same two clonal line B pupae, one wild type and one transgenic, imaged under bright field (left) and epifluorescence, with filters set to detect GCaMP6s (middle) and dsRed (right). Pupae were imaged 10 days after pupation.
- (B) Anti-dsRed (magenta) labels the ALs, indicating co-expression of dsRed with GCaMP6s (green; endogenous fluorescence) in ants carrying (*ie1-dsRed*, *ObirOrco-QF2*, *15xQUAS-GCaMP6s*). Phalloidin stains actin (cyan).
- (C) GCaMP6s fluorescence (green) is detectable in the subesophageal zone (SEZ).
- (D) GCaMP6s fluorescence (green) is also visible in processes innervating part of the central complex (CC), as well as in a nearby cluster of somas. Images show max z-projections through the imaged brain regions.
- (E) After unilateral ablation of the antenna (from the scape), bilaterally symmetrical GCaMP6s signal is still detectable in the central complex (CC), as well as the subesophageal zone (SEZ). No anti-Orco signal was detected in these brain regions. Images show max z-projections through the imaged brain regions.

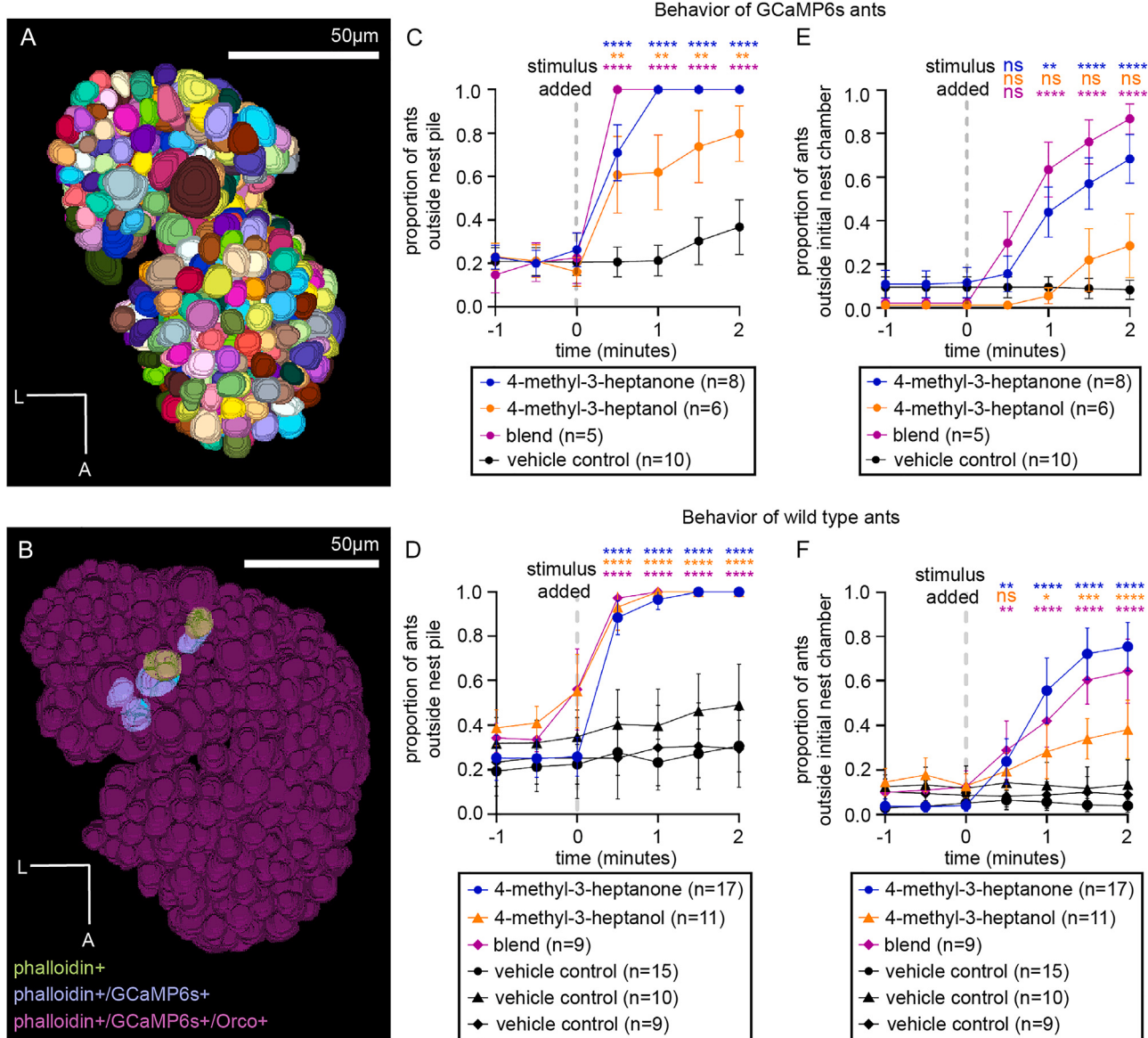


Figure S2. GCaMP6s ants have normal antennal lobes and respond to alarm pheromones, related to Figures 1 and 2

(A) 505 glomeruli reconstructed from the right AL of a GCaMP6s ant using anti-SYNORF1 staining.

(B) 508 glomeruli reconstructed from the left AL of a GCaMP6s ant using GCaMP6s signal, anti-Orco staining, and phalloidin staining. 502 glomeruli stained positive for phalloidin, GCaMP6s, and Orco; 4 glomeruli stained positive for phalloidin and GCaMP6s, but not Orco; and 2 glomeruli stained positive for phalloidin, but not GCaMP6s and Orco. The AL in (B) comes from a different ant than that in (A) and is shown in mirror image to align more closely with the image in (A).

(C–F) Colony alarm bioassay, showing mean \pm SEM. (C and D) GCaMP6s ants and wild-type ants leave the nest pile in response to 4-methyl-3-heptanone, 4-methyl-3-heptanol, and a 9:1 blend of the two compounds. (E and F) GCaMP6s ants and wild-type ants leave the nest chamber in response to 4-methyl-3-heptanone and the blend; wild-type ants also leave the nest chamber in response to 4-methyl-3-heptanol, whereas this response was not statistically significant in the GCaMP6s ants. Analyses for wild-type ants (D and F) are based on previously published data (Figure 3, 2,600 μ g and vehicle control treatments in Lopes et al.²²). For the experiment in GCaMP6s ants (C and E), all pheromone treatments were compared with the same set of vehicle control trials. For the experiments in wild-type ants (D and F), each pheromone treatment was conducted alongside its own set of vehicle control trials. Treatments and controls from the same experiment were statistically compared with each other and are plotted using identical symbol shapes. *p < 0.05, **p < 0.01, ***p < 0.001, ****p < 0.0001. L, lateral; A, anterior.

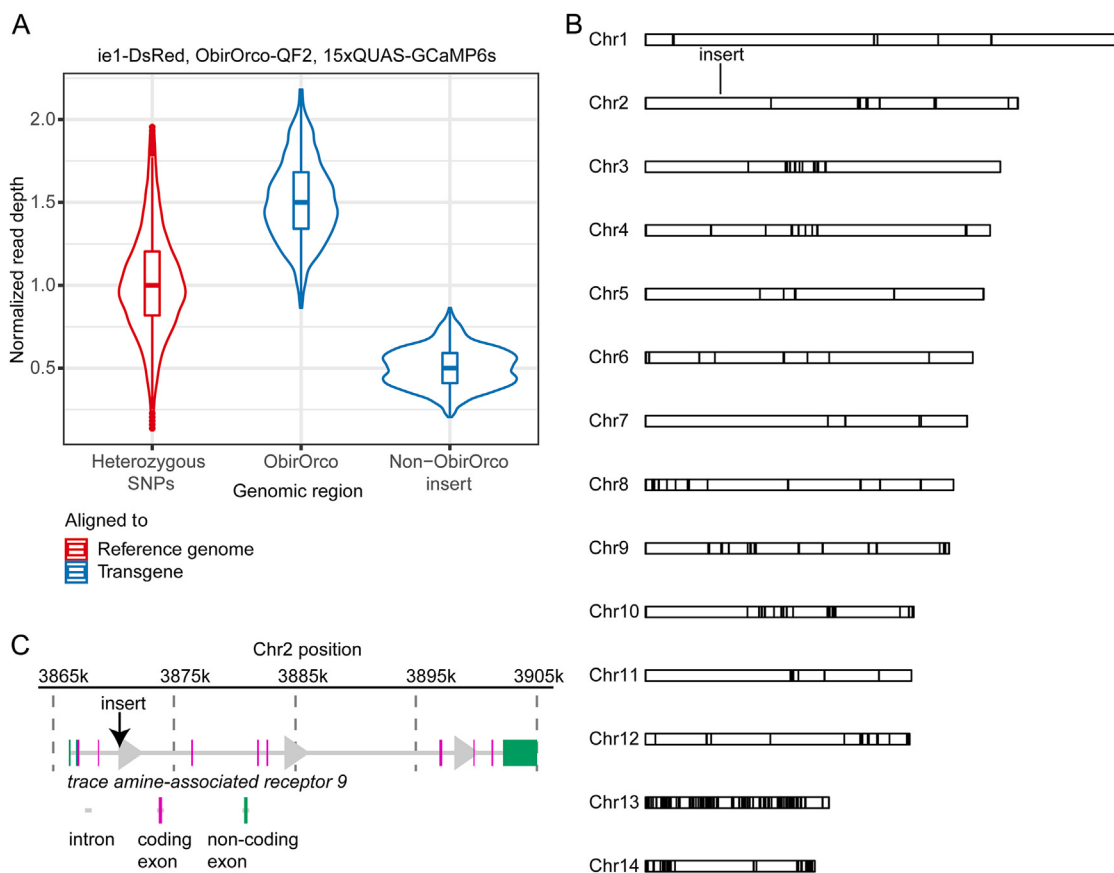
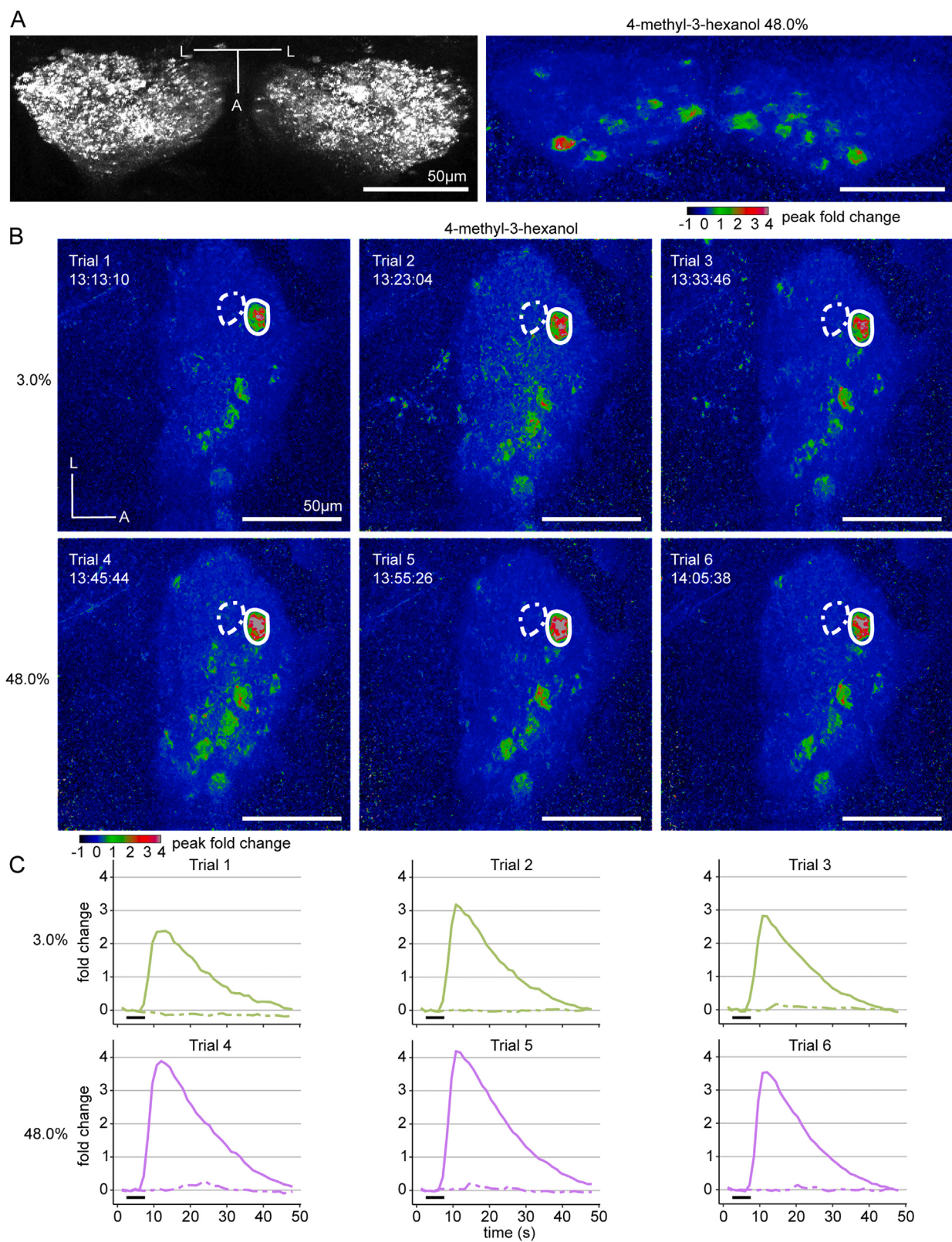


Figure S3. Genomic analyses of the transgenic line used for imaging, related to Figure 2

(A) Normalized read depth for reads aligning to a panel of heterozygous SNPs, the ObirOrco promoter, and the non-ObirOrco portion of the transgene. Normalized read depth for ObirOrco is ~1.5, corresponding to a single additional copy of ObirOrco inserted into the genome (added to the two endogenous copies). Normalized read depth of ~0.5 at the rest of the insert is also consistent with a single copy (haploid) insertion.

(B) The transgene insert was localized to a site on the 2nd chromosomal scaffold. Black bars indicate breaks between contigs.

(C) Close up of the transgene insertion locus within an intron of the gene *trace amine-associated receptor 9*.



(legend on next page)

Figure S4. Calcium responses are bilaterally symmetrical and remain robust across trials, related to Figure 4

(A) Max z-projections of both antennal lobes, imaged bilaterally. Both in raw fluorescence (left) and peak fold change of calcium response to presentation with 4-methyl-3-hexanol (right), the antennal lobes appear bilaterally symmetrical.

(B) Max z-projections of peak fold change from a single ant after presentation with 4-methyl-3-hexanol. Three trials were performed at 3.0% concentration (top), and three additional trials were performed at 48.0% concentration (bottom). Timestamps for each trial demonstrate that responses are robust over the duration of a full experiment. Two adjacent focal glomeruli are circled.

(C) Time series of calcium responses from each trial in (B) for the two adjacent glomeruli; responses in the left glomerulus are shown as alternating short and long dashes and responses in the right glomerulus are shown as solid lines; black bars indicate the 5 s odor presentations. Responses are quantified from max z-projections of three slices centered on 105 μm z-depth. L, lateral; A, anterior.

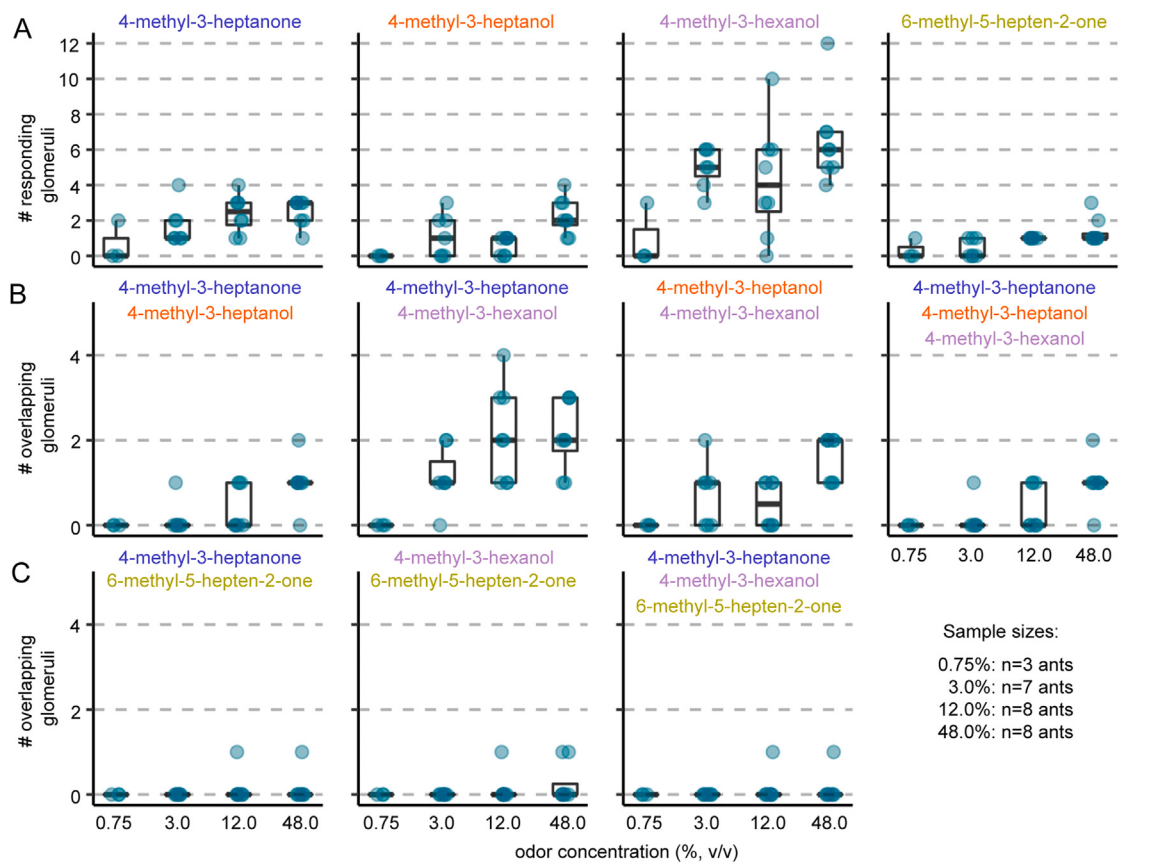


Figure S5. Increased odor concentration results in more responding glomeruli, related to Figures 4 and 5

Counts of the number of responding glomeruli from max z-projections; boxes enclose the first to third quartile range, with bold line showing the median and whiskers enclosing the min and max values that fall within $1.5 \times$ the interquartile range. Data points show the mean number of responding glomeruli for a given ant across all trials for a particular odorant/concentration. n = 13 ants total, 3 ants presented with 0.75% and 12.0% odor concentrations; 2 ants with 3.0% and 12.0%; 3 ants with 12.0% and 48.0%; and 5 ants with 3.0% and 48.0%. Single pheromones each activated a small number of glomeruli (A), and 4-methyl-3-heptanone, 4-methyl-3-heptanol, and 4-methyl-3-hexanol activated overlapping sets of glomeruli (B). 6-methyl-5-hepten-2-one only rarely activated glomeruli shared with the other pheromones (C). All pheromones were presented separately, rather than as blends. Only pheromones and pheromone combinations that activated at least one glomerulus are shown.

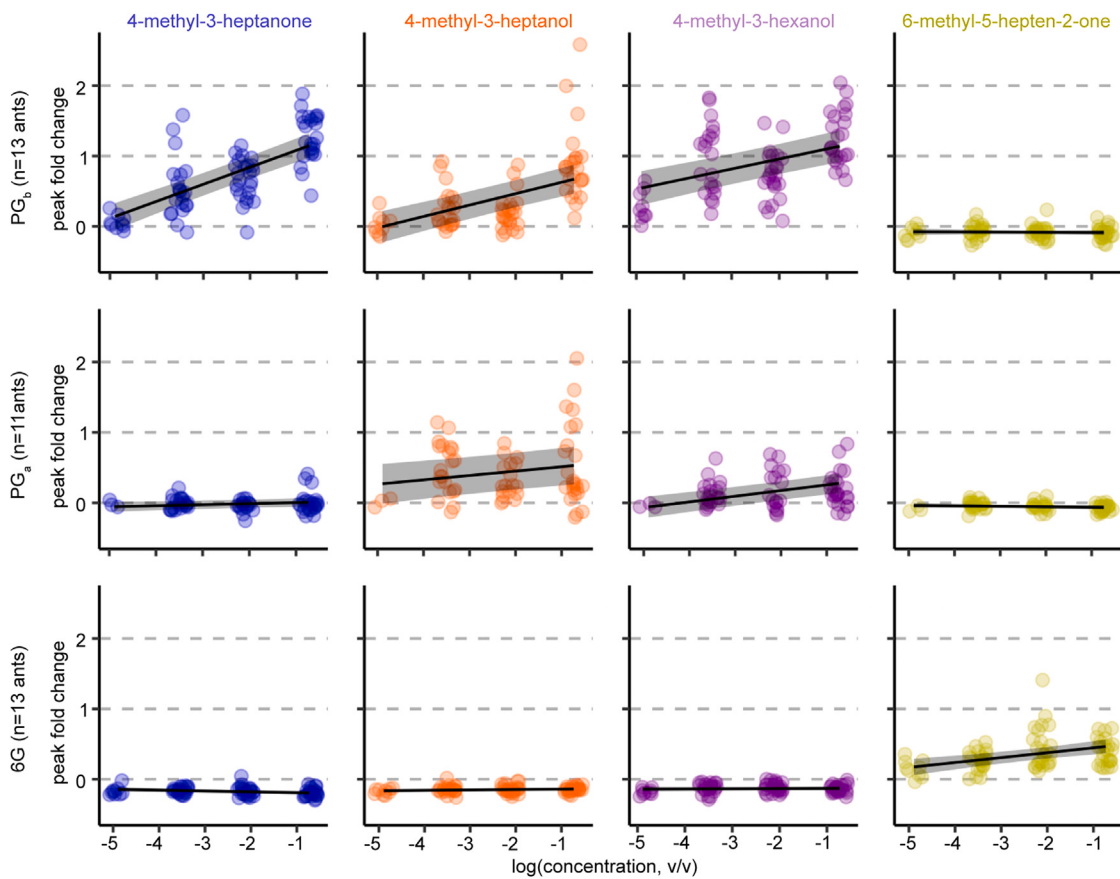


Figure S6. Quantification of peak fold change in PG_b (top), PG_a (middle), and 6G (bottom), related to Figure 5

Three trials per ant for each odorant/concentration; n = 13 ants total, 3 ants presented with 0.75% and 12.0% odor concentrations; 2 ants with 3.0% and 12.0%; 3 ants with 12.0% and 48.0%; and 5 ants with 3.0% and 48.0%. PG_a could not be identified in two ants. Graphs show outputs of linear models (with 95% confidence intervals) for dose/response to each odorant in each glomerulus, with a random effect for individual. Concentrations were log transformed to show the linear relationship.

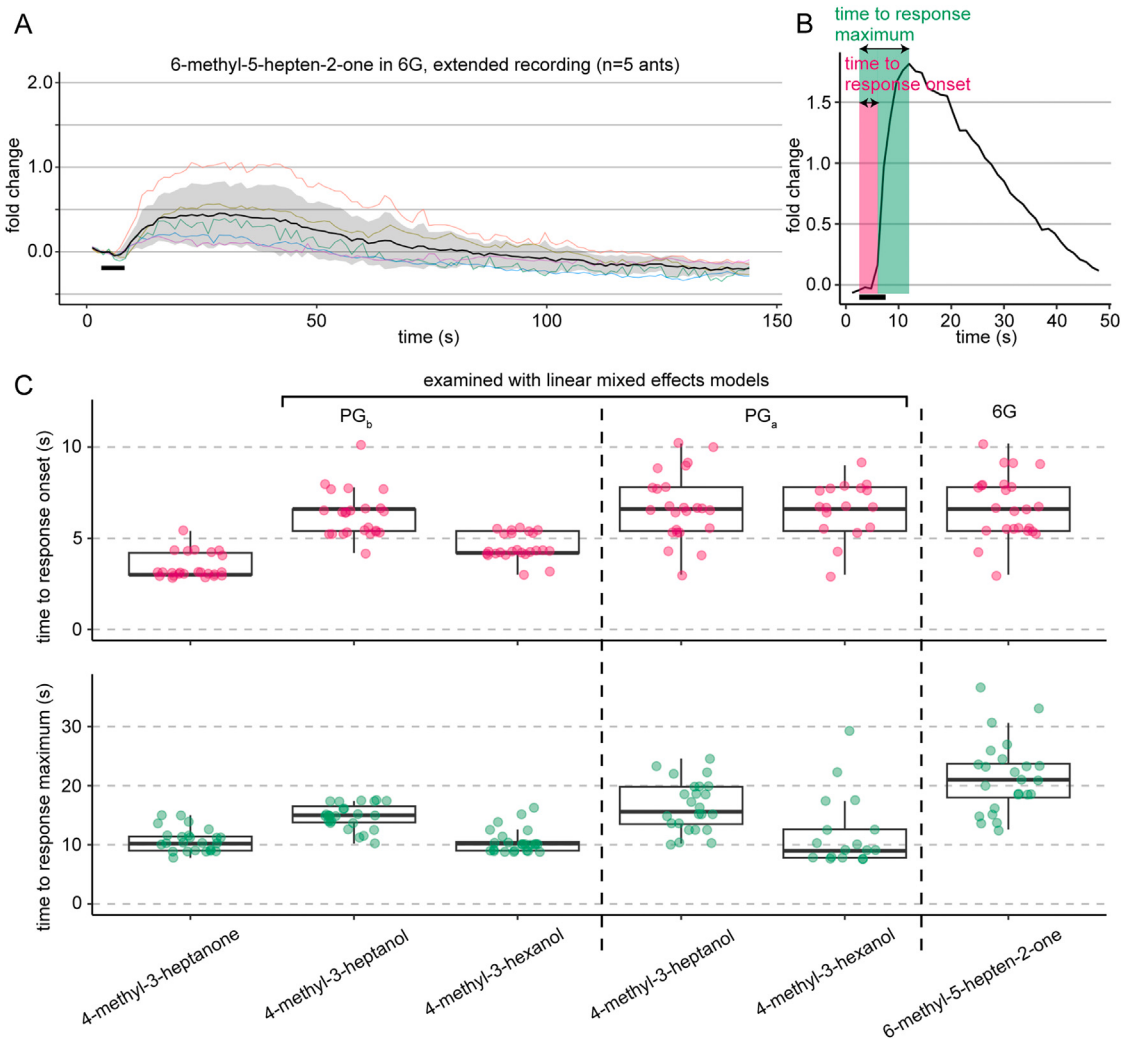


Figure S7. Temporal dynamics in three focal glomeruli, related to Figure 5

(A) Extended time series for the response to 6-methyl-5-hepten-2-one in 6G. Data were collected separately from Figure 5C. Shown are single trials each from five different individuals at 48% concentration (colored traces); mean \pm SD (black line and gray ribbon). Fluorescence plateaued for \sim 30 s before declining and returning to baseline \sim 80 s after odor presentation.

(B) Two parameters of temporal dynamics extracted from glomerulus-specific calcium response traces.

(C) Quantification of time to response onset (top) and time to response maximum (bottom) in the three focal glomeruli PG_b, PG_a, and 6G in response to stimuli at 48% concentration (n = 8 ants, three trials per condition per ant). Only glomerulus/pheromone combinations with typically robust responses are shown. Boxes enclose the first to third quartile range, with bold lines showing the median and whiskers enclosing the min and max values that fall within 1.5 \times the interquartile range. For PG_b and PG_a responses to 4-methyl-3-heptanol and 4-methyl-3-hexanol, we used linear mixed effects models to test for effects of pheromone, glomerulus, and a pheromone/glomerulus interaction on the time parameters. Time to response onset: significant effects of pheromone (p = 0.0034), glomerulus (p < 0.0001), and the interaction (p = 0.0030). Time to response maximum: significant effects of pheromone (p < 0.0001) and glomerulus (p = 0.047), but not the interaction (p = 0.88).